Erasing motion: Scrambling direction selectivity in visual cortex during saccades

Satoru K. Miura[1,2,3] & Massimo Scanziani[1,2,3]

1. Center for Neural Circuits and Behavior, Neurobiology Section and Department of Neuroscience, University of California, San Diego, La Jolla, CA, USA

2. Department of Physiology, University of California, San Francisco, San Francisco, CA, USA

3. Howard Hughes Medical Institute, University of California, San Francisco, San Francisco, CA, USA

Abstract

A prominent feature of sensory processing is the ability to distinguish whether the activation of the sensory periphery is caused by changes in the external world or by the animal's own actions[1]. Saccades, rapid eye movements executed by animals across phyla[2–4], cause the visual scene to momentarily shift on the retina. The mechanisms by which visual systems differentiate between motion of the visual scene induced by saccades from motion due to changes in the external world are not fully understood. Here, we discovered that in mouse primary visual cortex (V1), the two types of motion evoke distinct patterns of activity across the population of neurons. As a result, a decoder of motion direction trained on the response to motion in the external world fails to generalize when tested on the response to saccades that induce similar motion on the retina. This is because during saccades, V1 combines the visual input with a strong non-visual input arriving from the pulvinar nucleus of the thalamus. This non-visual input is an efference copy – a copy of the oculomotor command that differs depending on the direction of the saccades. Silencing the pulvinar prevented the non-visual input from reaching V1, such that the pattern of activity in V1 was now similar no matter whether the motion was generated in the external world or by saccades. Thus, the pulvinar input to V1 ensures differential responses to the external and self-generated motion and may prevent downstream areas from extracting motion information about visual stimulus shifts generated by saccades. Changing the pattern of evoked activity through an efference copy may be a general mechanism that enables sensory cortices in mammals to distinguish between external and self-generated stimuli.

Main

The sensory periphery is often stimulated by the animal's own movements, and nervous systems have evolved mechanisms to distinguish those stimuli from externally generated ones[1]. Prime examples are saccades, rapid eye movements that induce a fast displacement of the visual scene on the retina. They are common in animals across phyla, including animals without fovea like rodents[2–4], and they contribute to shifts of the gaze. Behavioral studies indicate that such saccade-induced motion of the visual scene is distinguished from motion occurring in the external world[5–10].

How visual systems distinguish the two types of motion has been a long-standing question. One factor that is believed to play a key role is a non-visual signal originating from saccade command centers called an efference copy, i.e., a copy of the oculomotor command[11,12]. This non-visual signal, occurring around the time of saccades, is believed to be transmitted to specific nodes along the visual pathway, where it interacts with the neural responses to saccade-induced motion of the visual scene. One model proposes that the non-visual signal suppresses the responses to the saccade-induced motion[13–16]. An alternative model proposes that it alters the pattern of the responses to the motion[17]. These models are not mutually exclusive, and indeed, in the mammalian visual cortex, studies have found evidence consistent with either model. In primary and higher visual areas, recordings show reduced responses to visual stimuli around the time of saccades[13,17–23], while altered neural representation of motion direction of the visual scene has been reported in areas associated with motion perception[17,18]. However, the origin of the non-visual signal to the visual cortex, what it encodes, and how it impacts the neural representation of the motion induced by saccades is not known. Here, we addressed these issues in V1 of mice.

Scrambling of direction preference in V1 during saccades

To assess whether neuronal activity in response to saccades differs from that in response to externally induced motion of the visual scene, we performed extracellular recordings across cortical layers in the monocular region of V1 in head-fixed, awake mice. We presented a stationary vertical sinusoidal grating on a monitor placed in the visual field contralateral to the recorded hemisphere and tracked the movements of the corresponding eye (Fig. 1a, b). We recorded the activity in response to shifts of the grating on the retina resulting from spontaneous saccades and compared it to the activity in response to pseudo-saccades. Pseudo-saccades are shifts of the grating on the monitor designed to approximate the shifts resulting from real saccades. Saccades occurred predominantly along the horizontal axis in either the nasal or temporal direction

consistent with previous reports[24,25] (Fig. 1c, d), had a frequency of 3.3 ± 0.3 saccades/min (nasal, 2.0 ± 0.2; temporal 1.3 ± 0.2), mean amplitude of 10.9 ± 1.9° (nasal, 13.1 ± 2.8; temporal, 7.5 ± 1.1; Extended Data Fig. 1), and mean 10 - 90% risetime of 23.0 ± 1.5 ms (nasal, 19.4 ± 1.7; temporal, 28.3 ± 3.1) resulting in average speed of 472 ± 100° /s [nasal, 601 ± 158; temporal, 274 ± 69; all stats average ± standard deviation (s.d.) of 4 mice].

The activity of the majority of V1 neurons (~60%) was significantly modulated within the first 100 ms from saccade onset (189 out of 317, 4 mice; see Methods for response criteria), leading to an average increase of activity across cortical layers (Extended Data Fig. 2). Furthermore, more than half of the responding neurons exhibited a significant preference for either nasal or temporal saccades (97 out of 189; Fig. 1e, f). Both the activity and the directional preference outlasted the saccade duration by several tens of milliseconds, as shown by the peri-event time histogram (PETH; Fig. 1f, right). Thus, saccades elicit strong, direction selective responses in V1. To compare the responses between real and pseudo-saccades, we presented pseudo-saccades with a rise-time of 25 ms and whose amplitudes (i.e., horizontal shift of the grating) ranged from 3.0° to 24.6° (see Methods). Shifts of the grating in the nasal direction were termed temporal pseudo-saccades because they generated a shift of the image on the retina in the same direction as that generated by real temporal saccades. Conversely, temporal shifts of the grating were termed nasal pseudo-saccades. For the analysis, we selected pseudo-saccades whose amplitudes and directions were matched to those of the real saccades performed by each animal during the recording session [average amplitude 10.9 ± 1.8° (nasal, 13.1 ± 2.7; temporal, 7.6 ± 1.0; Extended Data Fig. 1), average speed 437 ± 73° /s (nasal, 522 ± 108; temporal, 303 ± 39; all stats average ± s.d. of 4 mice); see Methods]. A large fraction of V1 neurons (50%, 157 out of 317) responded to pseudo-saccades, and 28% of these neurons (44 out of 157) showed a preference for the nasal for temporal direction (Fig. 1g, h; Extended Data Fig. 2).

Given the response of neurons to pseudo-saccades, the observed saccade-induced activity could simply result from the shift of the grating on the retina. If this is the case, we should expect a correlation between the direction preference of neurons to saccades and pseudo-saccades. For instance, a neuron that preferentially responds to nasal saccades should also prefer nasal pseudo-saccades, given that both result in the same temporal shift of the grating from the perspective of the animal's eye. In marked contrast to this expectation, there was a lack of correlation between the direction preference to real and pseudo-saccades of V1 neurons [Pearson correlation coefficient (ρ) = 0.22, p = 0.14, n = 44; Fig. 1j, k]. Among the neurons that discriminated the direction of pseudo-saccades, in response to real saccades, 41% reversed

direction preference (18 out of 44), and for the rest of the neurons, direction selectivity was decreased or enhanced, irrespective of the pseudo-saccade direction preference and selectivity (Fig. 1j, k). Furthermore, among the neurons that respond but did not discriminate the direction of pseudo-saccades, 35% became direction selective in response to real saccades (40 out of 113; Extended Data Fig. 3). Thus, saccades and pseudo-saccades induce distinct patterns of activity in V1. Furthermore, the response of V1 neurons to saccades are unlikely to solely result from the shift of the visual scene on the retina.

Despite the poor correlation between the response to real and pseudo-saccades, the probability distributions of direction preference was similar, as if direction preference had been randomly reassigned using the original probability distribution (22 out of 44 prefer nasal saccades, 18 out of 44 prefer nasal pseudo-saccades; Z-test, $p = 0.39$). We therefore refer to the impact of saccades on direction preference as “scrambling”.

Given the poor correlation between the response to real and pseudo-saccades, a decoder of motion direction (i.e., nasal or temporal) trained on V1 population response to pseudo-saccades should be unable to generalize to the response to real saccades. Indeed, while such a linear classifier was able to decode the direction of pseudo-saccades at a level well above chance, the accuracy fell close to chance for real saccades (72.6 ± 0.6% accuracy ± s.e.m. for pseudo-saccades, 56.2 ± 0.1% for real saccades, with 250 units; Wilcoxon rank-sum test, one-tail, $p < 0.0001$, $n = 50$ for pseudo-saccades, 50 for real saccades; see Methods; Fig. 1l). These results show that saccades scramble direction selectivity in V1, thereby impairing the decoding of direction of saccade-induced visual motion by a classifier tuned for external motion.

V1 receives non-visual input during saccades

Why is the response of V1 neurons to real saccades so different from the response to pseudo-saccades? We hypothesized that, around the time of saccades, a non-visual signal enters V1 thereby interfering with the visual signal arriving from the retina. Consistent with this hypothesis, in neurons showing saccade direction preference, the PETHs for preferred and non-preferred saccade directions diverged as early as 220 ms before the saccades [200 ms window before onset, 1.1 ± 0.2 Hz evoked firing rate (*fr*) ± s.e.m. for the preferred direction, -0.6 ± 0.2 Hz for the non-preferred; Wilcoxon signed-rank test, one-tailed, $p < 0.0001$, $n = 97$; Fig. 1f, right]. Given that the modulation of V1 activity occurs before the saccadic eye movement, it cannot be accounted for by a change in the visual scene on the retina, suggesting the presence of a non-visual signal.

To isolate this putative non-visual signal, we used two different approaches, both aimed at preventing changes in visual input during saccades. We recorded the response of V1 neurons to saccades made either in front of a gray screen (i.e. a visual scene where the luminance is homogeneous in space; Fig. 2a, b) or with tetrodotoxin (TTX) injected in both eyes to block retinal activity (Fig. 2c, d, Extended Data Fig. 1). In both cases, saccades still triggered strong, directionally selective responses in V1. With the gray screen, 55% of all neurons responded to saccades, of which 63% discriminated the direction, thus resembling saccades made on the vertical grating (174 responsive, 109 discriminating out of 317 total, 4 mice; Fig. 2a, b). Furthermore, the PETH for the preferred and non-preferred directions diverged prior to saccade onset (200 ms window before onset, 0.2 ± 0.1 Hz evoked *fr* ± s.e.m. for preferred, -0.1 ± 0.03 Hz for non-preferred; Wilcoxon signed-rank test, one-tailed, $p < 0.0001$, $n = 109$; Fig. 2b, right). Similarly, in TTX-blinded animals, about half of the neurons in V1 responded to saccades, of which 64% discriminated the direction (100 responsive, 64 discriminating out of 203 total, 8 mice; Fig. 2c, d, Extended Data Fig. 4), and the PETH for the preferred and non-preferred directions diverged well before saccade onset (200 ms window before onset, 1.0 ± 0.3 Hz evoked *fr* ± s.e.m. for preferred, -0.4 ± 0.2 Hz for non-preferred; Wilcoxon signed-rank test, one-tailed, $p = 3.3 \times 10^{-4}$, $n = 64$; Fig. 2d, right). The block of visual input in TTX-blinded animals was verified by the complete absence of responses in V1 to visual stimuli (Extended Data Fig. 5). This complete block of visual input allowed us to estimate the site of the non-visual input entry using the local field potential (LFP). The current source density analysis of the saccade triggered LFP revealed a strong sink in the superficial layers of V1, making this site a likely entry point of the non-visual input (Extended Data Fig. 4). These data demonstrate that mouse V1 receives a non-visual input that carries saccade direction information.

To determine how the non-visual and the visual inputs interact in V1 during a saccade, we made a simple model based on linear regression. We used the responses to saccades in front of the gray screen as a proxy for the non-visual input and the responses to pseudo-saccades as a proxy for the visual input to predict the response to saccades made in front of a vertical grating. We based this analysis on 79 neurons that responded to both saccades on a gray screen and to pseudo-saccades (4 mice; Fig. 2e). There was no correlation between the direction selectivity of these neurons to saccades on a gray screen and pseudo-saccades, indicating that the direction selectivity imparted by the visual and non-visual inputs to V1 neurons are independent (Pearson $\rho = 0.024$, $p = 0.84$, $n = 79$; Fig. 2f). Using a simple summation of the visual and non-visual inputs, this model explained 83% of the variance of the saccade response in front of a vertical grating

(Fig. 2g). The estimated gain on the combined input was 0.61 ($p < 0.0001$), suggesting a linear integration with a gain reduction. In contrast, when using only the response from visual or from the non-visual inputs, the model explained only 32% or 69% of the variance, respectively (Extended Data Fig. 6). Taken together these data suggest that the scrambling of the direction selectivity during a saccade results from the integration of visual and non-visual inputs whose direction selectivity are uncorrelated. To test this hypothesis, we proceeded to identify the source of the non-visual input. Silencing this source should eliminate the non-visual signal in V1 and prevent the scrambling of direction selectivity during saccades.

The pulvinar nucleus provides non-visual input to V1 during saccades

What is the source of the non-visual saccadic input to V1? We recorded from the dorsolateral geniculate nucleus of the thalamus (dLGN), the main source of afferent visual information to V1, to determine whether it is also the source of the non-visual input. Neurons in this structure have been shown previously to respond to saccades[26–29]. In TTX-blinded animals, dLGN neurons responded to saccades and their responses were selective for saccade direction (83 responsive, 49 discriminating, 174 total, 4 mice; Fig. 3a, Extended Data Fig. 7). We thus silenced the dLGN with muscimol injection in otherwise un-manipulated (i.e., non-blinded) animals. In contrast to the lack of visual responses in V1 confirming efficient silencing of the dLGN (Extended Data Fig. 8), V1 neurons still robustly responded to saccades and discriminated the two directions (106 responsive, 56 discriminating, total 139, 4 mice; Fig. 3b, Extended Data Fig. 7). These data show that the dLGN is not the main source of non-visual saccade input to V1.

We next focused on the pulvinar, a higher-order thalamic nucleus with extensive projections to superficial layers of V1[30], consistent with the estimated entry point of the non-visual input (see above), and a structure in which neurons have also been shown to respond to saccades[29,31]. Indeed, recordings in the pulvinar in TTX-blinded animals revealed that almost half of the neurons responded to saccades (102 out of 225, 12 mice), many of which were also direction selective (61 out of 102; Fig. 3c, d). Furthermore, the PETH of directionally selective pulvinar neurons for the preferred and non-preferred directions diverged prior to saccade onset (200 ms window before onset, 0.7 ± 0.2 Hz evoked *fr* ± s.e.m. for the preferred direction, 0.2 ± 0.2 Hz for the non-preferred; Wilcoxon signed-rank test, one-tailed, $p = 0.013$, $n = 61$; Fig. 3d, right). We also verified that some of these neurons directly project to V1, using Channelrhodopsin-2 mediated antidromic activation[32–34] (see Methods for detailed protocol and criteria). Of 23 neurons that were identified in such a manner, more than half responded to saccades (13 out of 23, 3 mice), while 5 neurons

discriminated the direction (Fig. 3e, f). We tested whether neurons in the pulvinar provide the non-visual saccadic input to V1 by silencing the pulvinar (using either TTX or muscimol), while recording from V1 in TTX-blinded animals (Fig. 3g). Consistent with the idea, pulvinar silencing abolished the non-visual saccadic response in V1 neurons (88 ± 19% average decrease ± s.e.m. in saccade evoked *fr*; Wilcoxon signed-rank test, one-tailed, $p = 0.012$, $n = 56$; based on 56 saccade responsive neurons out of 140 pre-silencing, 5 mice) as well as the saccade mediated response in the LFP (Fig. 3g, h, Extended Data Fig. 9). The silencing also strongly reduced the ability of V1 neurons to discriminate saccade directions (pre-silencing, 6.8 ± 1.6 Hz difference in evoked *fr* ± s.e.m. between preferred and non-preferred; post silencing, 1.3 ± 0.6 Hz, 74 ± 11% reduction; Wilcoxon signed-rank test, one-tailed, $p < 0.0001$, $n = 29$; based on 29 neurons that discriminated pre-silencing, 5 mice; Extended Data Fig. 9). Taken together, these results demonstrate that the pulvinar is the main source of the non-visual saccade input to V1.

The pulvinar input scrambles direction selectivity in V1

If the pulvinar is the main source of the non-visual input, silencing it should lead to saccade responses in V1 that are mainly visual, driven by the shift of the image on the retina. In other words, pulvinar silencing should prevent scrambling, resulting in similar direction preference for real and pseudo saccades. We thus recorded the activity of V1 neurons in response to saccades made on the vertical grating, after injecting muscimol in the pulvinar, and compared it to the response to pseudo-saccades (Fig. 4a, b, Extended Data Fig. 1). Strikingly, with pulvinar silencing, direction selectivity for real saccades became correlated with that for pseudo-saccades (Pearson $\rho = 0.72$, $p < 0.0001$, $n = 29$, 9 mice; Fig. 4c; a similar correlation was obtained also when including neurons lacking direction selectivity to pseudo-saccades; Extended Data Fig. 3). That is, the response of V1 neurons to a stimulus shifting on the retina was similar no matter whether the motion was induced externally or by eye movement. Consistent with the correlation in the direction selectivity, the classifier trained on pseudo-saccades was able to decode the directions of saccade-induced visual motions at the level of performance indistinguishable from pseudo-saccades (74.2 ± 0.7% accuracy ± s.e.m. for pseudo-saccades, 73.3 ± 0.7% for real saccades with 250 units; Wilcoxon rank-sum test, two-tail, $p = 0.34$, $n = 50$ for pseudo-saccades, 50 for real saccades; Fig. 4d). Thus, the pulvinar provides a saccade triggered non-visual input that scrambles direction selectivity in V1 (Fig. 4e).

Discussion

Our study revealed that the response to external motion and saccades can be readily distinguished as early as in V1. This is because, during saccades, V1 combines the visual input originating from the retina with a non-visual input originating from the pulvinar. The combination of the visual and non-visual inputs scrambles direction preference of V1 neurons. As a consequence, the activity pattern in V1 in response to an image moving on the retina differs depending on whether that motion was generated by the motion of the external world or the motion of the retina. The scrambling during saccades may prevent downstream areas from decoding the direction of visual motion induced by the animal's own saccadic eye movement.

The scrambling of direction preference of V1 neurons relies on the fact that the non-visual input is itself directionally selective yet its direction preference does not correlate with that of V1 neurons to visual input. This strategy to distinguish between motion in the external world from self-generated motion may be advantageous relative to a hypothetical suppression of V1 during a saccade: On one hand, recovery from total inhibition in highly recurrent networks such as the visual cortex, is slow while, on the contrary, visual sensitivity has been shown to increase after saccades[21,35]. On the other hand, selective inhibition of neurons with a specific direction preference would require a highly precise connectivity between the pulvinar and V1. The strategy employed by the mouse visual system presents a simple yet effective solution to briefly change the representation of visual motion during saccades. Furthermore, given that the pulvinar input contains information about eye movement direction, the integration with the visual input may represent sensorimotor integration for estimation of the state of the eye such as its position and velocity. Such an estimator has recently been invoked in a theoretical study of eye movement control[36]. Thus, the pulvinar input may serve functions beyond scrambling of direction selectivity during saccades.

Because V1 activity is modulated by an upcoming saccade, i.e. before saccade onset, the non-visual input from the pulvinar must be, at least in part, a copy of the oculo-motor command, or an efference copy. The fact that the pulvinar receives substantial input from the superior colliculus[37,38], a midbrain structure involved in saccade initiation, further supports this hypothesis, yet we cannot exclude that later parts of the non-visual input may reflect proprioceptive signals originating in the eye muscles.

In humans, motion on the retina induced by saccades is often perceptually unnoticed, a phenomenon termed saccade suppression. Despite the lack of perceptual experience, however, studies in humans show that visual processing remains active during saccades[39,40]. These results are consistent with our finding that there is no complete suppression of V1 activity and that the

visual signal, rather than being eliminated, is combined with the non-visual input. Furthermore, our model suggests that the gain of the visual signal is reduced during saccades, consistent with the notion that saccade suppression could be contributed by a reduction in gain[41].

Previous research in primate V1 have generally found modest responses to saccades in the absence of visual stimuli or in darkness, and the change of direction preference has been reported only in higher visual areas[19,35,42–47]. While the primate and rodent visual systems may use different strategies to distinguish between external and self-induced motion, the difference may also reflect the distinct cortical hierarchies across species[48], whereby V1 in mice encompasses functions found only in higher visual areas in primates.

In conclusion, we have uncovered the circuit mechanism that allows the visual system to distinguish motion induced by the animal's own eye movement from changes in the external world. This mechanism, together with other visual and non-visual phenomena that occur within or upstream of visual cortex[49–51], may underlie the suppression of motion percepts induced by saccades.

Methods

Mouse handling

Experiments were conducted in accordance with the regulations of the Institutional Animal Care and Use Committee of the University of California, San Diego and of the University of California, San Francisco. All mice used in this study were wild-type C57BL/6J males or females from the Jackson Laboratory (JAX #000664) and between postnatal ages of three to six months.

Animals were habituated to head-fixation for at least two weeks prior to recording. During this time, they were also habituated to visual stimuli that would be used during recording. Animals were head-fixed on a custom-made passive treadmill, either circular or linear, and were free to run. The frequency of saccades was monitored for each animal during the habituation, and only the animals with relatively high frequency were selected for recording.

Eye tracking

Video-oculography was used to track the movement of the right eye, contralateral to the hemisphere in which recordings were conducted. A high-speed camera (IMPERX, IPX-VGA-210-L) was fitted with a 45 mm extension tube, a 50 mm lens (Fujifilm, Fujinon HF50HA-1B), and an infrared (IR) pass filter (Edmund Optics, #65-796). Images were acquired at 200Hz through a frame grabber (National Instrument, PCIe-1427). An IR hot mirror (Edmund Optics, #43-958) was placed parallel to the antero-posterior (A-P) axis of the animal (1 inch from the eye) in between the animal and the LCD monitor, and the camera captured the image of the eye through its reflection. The camera was angled at 59° relative to the A-P axis. Three IR 880 nm LED emitters (Digi-Key, #PDI-E803) were used to illuminate the eye, one of whose corneal reflection served as a reference for calculating the pupil position. The pupil was identified by thresholding and fitting an ellipse to determine the center. Angular position of the pupil was then calculated in relation to the corneal reflection of the reference LED, which was placed along the optical axis of the camera. The core component of the eye-tracking software has been published previously[52], and it was used with some modifications to fit this particular study.

Surgery

For head-fixation, mice were implanted with either a custom T-shaped head bar or three threaded screw inserts arranged in a triangle (McMaster-Carr, #92395A109). The implantation was done stereotactically using an inclinometer (Level Developments, DAS-30-R) connected to an USB I/O device (National Instruments, USB-6008), so that the axes of the electrode manipulators would

be aligned to the A-P, medio-lateral, and dorso-ventral axes of the skull. Mice were anaesthetized with 1.5% isoflurane and kept on a feedback regulated heat pad to maintain body temperature at 37 °C (FHC 40-90-8D). Prior to surgery, mice were given buprenorphine subcutaneously. Prior to incision, topical lidocaine cream was applied to the skin. Once the scalp and fascia were removed, the head bar or the screw inserts were cemented using dental cement (Lang Dental, Ortho-Jet for head bars; 3M ESPE, Relyx Unicem2 for screw inserts). The animals were allowed to recover in their home cage for at least 1 week following the surgery.

For the identification of pulvinar neurons that send projections to V1 through optogenetic antidromic activation, AAV2/1.hSyn.ChR2(H134R)-eYFP.WPRE.hGH (Addgene 26973P) was injected in the pulvinar in the left hemisphere, prior to the implantation of the head bar or screw heads.

Cranial windows for extracellular recordings were made one day prior to the recording sessions. For all recordings, the size was ~500 μm – 1 mm by ~500 μm – 1 mm. Whiskers that would interfere with eye tracking were also trimmed at this point. Following the craniotomy, the window was sealed with biocompatible silicone sealant until the recording session (World Precision Instruments, Kwik-Cast). The cranial windows were centered around the following coordinates that were marked during the head bar or screw insert implantation:

V1 recording: 2.7 mm lateral to the midline, 4.1 mm posterior to the Bregma

Pulvinar recording: 1.2 mm lateral to the midline, 1.9 mm posterior to the Bregma

dLGN recording: 2.4 mm lateral to the midline, 2.2 mm posterior to the Bregma

Visual stimulation

Visual stimuli were presented on an LCD monitor running at 240 Hz (Gigabyte, AORUS KD25F) to the right eye, contralateral to the hemisphere in which recordings were performed. The monitor was angled at 31° counterclockwise relative to the A-P axis of the animal and tilted 20° towards the animal relative to the gravitational axis. It was positioned such that the tangent point between the monitor and a sphere around the center of the eye was in the center of the monitor. The distance from the center of the eye to the tangent point was 133 mm. In one experiment described in Extended Data Fig. 5, an LCD monitor running at 75 Hz was used. Mean luminance of visual stimuli were between 40 to 60 cd/m^2 (gamma corrected; a fixed luminance for each animal), except for Extended Data Fig. 5 where the full-field flash was a change in mean luminance from 0 to 100 cd/m^2.

The static vertical grating used in the experiments described in Fig. 1 and 4 was a full-field sinusoidal grating with 70% contrast and spatial frequency of 0.08 cycles per degree (cpd). It was spherically morphed around the center of the animal's right eye to maintain the same spatial frequency across different spatial locations on the retina. For pseudo-saccades, the exact same grating was quickly shifted horizontally once every 1.5 seconds on average, over the span of 7 frames (6 inter-frame intervals, 25 ms). The speed of the shift over the 7 frames was linear. The direction and amplitude of each shift was pre-determined by randomly drawing from the distribution of real saccades collected separately from wildtype unmanipulated mice. For a nasal pseudo-saccade, the grating was shifted in the temporal direction, and for a temporal pseudo-saccade, the grating was shifted in the nasal direction. *Post-hoc*, every pseudo-saccade was checked for display errors such as a dropped frame. All pseudo-saccades that occurred within 500 ms of a real saccade were also discarded from further analyses, which resulted in about 350 pseudo-saccades for each animal over the span of 10 min. We then resampled the pseudo-saccades to match the direction and amplitude of the real saccades collected from the same animal. In order to increase the statistical power, we resampled two matching pseudo-saccade events for every saccade. The mean ± standard deviation of the difference in amplitude between a real saccade and its matched pseudo-saccades was 0.25 ± 0.45° (498 pseudo-saccades, 4 mice) for experiments in Figure 1 and 0.18 ± 0.45° (942 pseudo-saccades, 9 mice) in Figure 4.

For every animal, response to pseudo-saccades was collected at the beginning of the experiment. Response to real saccades using the static grating was collected after the pseudo-saccade session. The two responses were collected separately, in order to maximize our chances of obtaining saccades whose responses were not contaminated by pseudo-saccade responses.

For the experiment described in Extended Data Figure 8, the grating was a vertical grating with average luminance 40 cd/m^2, spatial frequency 0.02 cpd, and contrast 0.5. The presentation lasted 32 ms and was flanked temporally by gray screen with the same average luminance. It was presented on average once every 10 s.

All visual stimulation protocols were custom written in LabVIEW (National Instruments) and MATLAB (Mathworks) using Psychophysics Toolbox 3[53–55].

Extracellular recording

All recordings in this study were performed on the left hemisphere. On the day of recording, animals were first head-fixed, and the Kwik-Cast sealant was gently removed. Artificial cerebrospinal fluid (ACSF; 140 mM NaCl, 2.5 mM KCl, 2.5 mM $CaCl_2$, 1.3 mM $MgSO_4$, 1.0 mM

NaH_2PO_4, 20 mM HEPES, and 11 mM glucose, adjusted to pH 7.4) was quickly applied to the craniotomy to prevent the exposed brain from drying. Different configurations of silicon probes were used over the course of the study: A2x32-5mm-25-200-177-A64 (NeuroNexus), A1x64-Poly2-6mm-23s-160-A64 (NeuroNexus), A1x32-Poly2-10mm-50s-177-A32 (NeuroNexus), and ASSY-77 H2 (Cambridge NeuroTech). Using a manipulator (Luigs & Neumann), the probes were slowly lowered to the recording site. For V1, probes were lowered to 1,000 μm from the pia; for the dLGN, 3,000 μm; and for the pulvinar, 2,900 μm. For recordings in the thalamus, the probes were painted with lipophilic DiI prior to the insertion visualization of the recording track. Successful targeting was verified *post-hoc*.

For optogenetic activation of the axon terminals of pulvinar neurons, a glass fiber-optic cable (960 μm core, NA = 0.63; Doric Lenses) connected to a 465 nm LED light source (Doric Lenses, #LEDC1-B_FC) was placed ~500 μm above the craniotomy on V1. The light source was driven by an LED driver (Thorlabs, #LEDD1B) at 1000 mA for 1 ms every 6 s for 10 min (100 trials).

Recordings were started 15 minutes after the insertion of the probes. Signals were sampled at 30 kS/s using 64 channel headstages (Intan Technologies, #C3315) combined with adapters (NeuroNexus, Adpt.A64-Omnetics32_2x-sm), connected to an RHD USB interface board (Intan Technologies, #C3100). The interface board was also used to acquire signals from photodiodes (TAOS, #TSL253R) placed on the visual stimulation monitor as well as TTL pulses used to trigger the eye-tracking camera and the LED. These signals were used during analyses to synchronize visual stimulus timings, video acquisition timings, and LED photo-stimulation timings with electrophysiological recordings. All raw data were stored for offline analyses. Occasionally, we recorded from the same animal on two successive days, provided no *in vivo* pharmacology was performed on the first day. In these instances, the craniotomy was re-sealed with Kwik-Cast after the first recording session. Recording quality was qualitatively similar for the two sessions. When required, brains were fixed in 4% paraformaldehyde (PFA) in phosphate buffer saline (PBS) overnight at 4 °C for histological analysis.

In vivo **pharmacology**

Intraocular injection of tetrodotoxin (TTX; 40 μM) was performed 2 hours prior to recording under isoflurane anesthesia. A typical procedure lasted less than five minutes. In order to prevent the pupil from fully dilating, which would make the eye tracking less accurate, carbachol (0.011% w/v) was co-injected. Immediately prior to the injection, a drop of proparacaine hydrochloride ophthalmic solution was applied to the eye as a local anesthetic (Bausch + Lomb, 0.5%). TTX

409 solution was injected intravitreally using a beveled glass micropipette (tip diameter ~50 μm) on a
410 micro injector (Nanoject II, Drummond) mounted on a manual manipulator. 1 μL was injected in
411 each eye, at the speed of 46 nL/s. In some animals, the injection solution also contained NBQX
412 (100 μM) and APV (100 μM). However, this did not affect the efficacy of the silencing of retinal
413 activity. The animals were head-fixed for recording following a 2-hour recovery period in the home
414 cage. The suppression of retinal activity was confirmed for every experiment by observing the
415 lack of response in visual cortex following a strong full-field flash of the LCD monitor.

416 *In vivo* silencing of the dLGN and pulvinar was performed by injecting 30 nL of 5.5 mM muscimol-
417 BODIPY at the speed of 300 nL/min, using a beveled glass pipette (tip diameter ~20 - 40 μm) on
418 a micro injector UMP3 with a Micro4 controller (World Precision Instruments). The injector was
419 mounted on a micromanipulator (Luigs & Neumann) for stereotactic injection. In two of the
420 pulvinar silencing experiments, TTX was used instead. The concentration of TTX was 60 μM, and
421 40 μL was injected at 40 μL/min. After the recording, brains were fixed in 4% PFA in PBS overnight
422 at 4 °C for histological analysis of BODIPY on the next day.

423 **Histology**

424 Anesthetized mice were perfused transcardially with 4% PFA in PBS (pH7.4). Brains were
425 removed and further post-fixed in 4% PFA in PBS at 4 °C overnight, after which the solution was
426 replaced with PBS. They were kept at 4 °C until they were coronally sectioned (100 μm sections)
427 with a vibratome. Sections were mounted in Vectashield mounting media containing DAPI (Vector
428 Laboratories H1500) and imaged with a camera (Olympus DP72) attached to an MVX10
429 (Olympus) stereoscope.

430 **Analyses**

431 **Detection of saccades**

432 Saccades were detected post-hoc from the eye tracking data, using a custom written algorithm in
433 MATLAB. First, from the raw eye position data, the algorithm searched for any event in which the
434 eye position jumped more than 0.75 degrees along the horizontal axis in one video frame (5 ms).
435 Next, in order to exclude noise, we discarded all events where the eye position did not move in
436 the same direction for at least 3 successive frames (15 ms). For the event to be considered a
437 saccade, the peak amplitude in either direction had to exceed 3 degrees. Further, in order to
438 eliminate influence from previous saccades, we only analyzed saccades that were isolated in time
439 with over 500 ms of stationary eye period preceding the events.

Unit isolation

Single units from extracellular recordings were isolated using KiloSort[56] and visualized using Phy for further manual merging and splitting. The quality of isolated units was assessed using refractory period violations and stability of amplitude. The depth for each unit was assigned according to the electrode site at which its amplitude was the largest. For V1 recordings, all units that exceed trough-to-peak time of 0.5 ms was assigned as regular-spiking neurons, while all others were assigned as fast-spiking neurons. Multi units were defined as the collection of all units that remained after excluding noise using Phy. In the main text, we refer to single units as simply neurons.

For this study, we focused on saccade-related activity. Nonetheless, we found single units in our recordings whose activity correlated with the stationary eye position ("eye-position units"), both in control and TTX-blinded animals. Because there was a correlation between the direction of saccades and the horizontal starting position of the eye (i.e., nasal saccades start from more temporal positions on average than temporal saccades), some of these units were thus capable of discriminating the direction of future saccades. While these units are interesting, they would introduce a confounder in the current study. For instance, such a unit would discriminate the two directions of saccade, even if a saccade did not evoke any response. Thus, single units whose baseline activity were significantly different between the two directions of saccades were excluded from this study. A detailed future study of these units will be reported elsewhere. The number of the excluded eye-position units, along with the total number of isolated single units for each experiment are detailed here:

Isolated single units from V1 recorded with a stationary grating, pseudo-saccades, or a gray screen without any manipulation (Fig. 1; Fig. 2a, b): 353 total single units (36 eye-position units), 4 mice.

Isolated single units from V1 recorded under TTX-blinding (Fig. 2c, d): 254 total single units (51 eye-position units), 8 mice.

Isolated single units from the dLGN recorded under TTX-blinding (Fig. 3a): 198 total single units (24 eye-position units), 4 mice.

Isolated single units from V1 recorded under dLGN silencing (Fig. 3b): 163 total single units (24 eye-position units), 4 mice.

Isolated single units from the pulvinar recorded under TTX-blinding (Fig. 3c, d): 261 total single units (36 eye-position units), 12 mice.

Isolated single units from V1 recorded under TTX-blinding and pulvinar silencing (Fig. 3g): 156 total single units (16 eye-position units, prior to pulvinar silencing), 5 mice.

Isolated single units from V1 recorded with a stationary grating with pulvinar silencing (Fig. 4a, b): 328 total single units (32 eye-position units), 9 mice.

The estimation of the cortical depth for each electrode channel was made based on the spontaneous firing rate (*fr*) across depth. Based on the channel with the highest spike rate and the increase preceding the peak, the beginning of layer 5 was assigned on each electrode (~125 μm more superficial to the peak). The depth of all other channels was determined in relation. Channels spanning 150 μm above layer 5 was assigned layer 4, and channels above layer 4 were assigned Layer 2/3. All channels from the beginning of layer 5 up to 200 μm below were considered layer 5, and everything below layer 6.

Response to saccades and pseudo-saccades

Units were considered responsive if it met either of the criteria: the number of spikes elicited within 100 ms after the onset is significantly different from the baseline for either nasal or temporal direction; or if the number of spikes were significantly different between nasal and temporal directions. Statistical significance was determined by rank-sum test, with a *p*-value cutoff of 0.05. The baseline was calculated as the number of spikes within a 100 ms window between -300 ms to -200 ms from the onset.

All reported responses in the main text are average *fr* within the 100 ms window after onset, unless otherwise noted.

Direction selectivity and discriminability

Direction selectivity of each single unit was calculated as the area under the receiver operating characteristics curve (AROC), linearly rescaled to the range from -1 to 1 (also known as the Gini coefficient). That is, DPref = 2*AROC – 1. The order was fixed, such that negative values indicate a preference for temporal saccades, and positive values indicate a preference for nasal saccades. Direction preference was defined as the sign of direction selectivity. To calculate the selectivity, the total number of spikes within the first 100 ms post saccade or pseudo-saccade onset from each event was used, without baseline subtraction. Discriminability was then defined as the

absolute value of the direction selectivity. Statistical significance of discriminability was calculated with a rank-sum test with a p-value threshold of 0.05.

Average PETH with baseline normalization

When generating average PETH with baseline normalization, neurons with baseline below 0.5 Hz were excluded to avoid substantial biases resulting from extremely low *fr*. The baseline of each neuron to saccades or pseudo-saccades was calculated using its mean activity 500 ms to 200 ms before the onset. For other visual stimuli, mean activity between -200 to 0 ms before the onset was used. Note that this process was applied for *visualization purposes only*, and all statistics such as the calculation of direction selectivity and the differences in evoked *fr* were performed on raw or baseline subtracted values of all relevant neurons, rather than baseline normalized values. Below, we report the number of neurons excluded from each panel for baseline normalization [Number of all relevant neurons (number of neurons with baseline < 0.5 Hz)]: Figure 1f, right: 97 (9); Figure 1h, right: 44 (11); Figure 2b, right: 109 (12); Figure 2d, right: 64 (4); Figure 3a: 49 (8); Figure 3b: 56 (9); Figure 3d, right: 61 (1); Figure 3f: 13 (0); Figure 3g, right, pre-silencing: 56 (6); Figure 3g, right, post-silencing: 56 (8); Figure 4a, center: 135 (12); Figure 4a, right: 53 (4); Figure 4b, center: 102 (10); Figure 4b, right: 29 (3); Extended Data Figure 9b: 29 (6).

Modeling of saccade response on vertical grating with visual and non-visual inputs

Saccade response on vertical grating (the number of evoked spikes within 100 ms from onset) was predicted from 1) pseudo-saccade response, 2) saccade response on gray screen, or both. All responses were baseline subtracted values. The model is linear regression (five-fold cross validated) with no intercept, followed by a nonlinear filter which made sure that the predicted *fr* did not fall below 0 Hz. That is, if the predicted decrease in evoked number of spikes exceeded the baseline *fr*, the value was adjusted so that the sum of the prediction and the baseline was zero. The explained variance is calculated as the Explained Sum of Squares divided by the Total Sum of Squares.

Identification of pulvinar neurons with axonal projections to V1 through antidromic activation

1 ms pulses (100 trials) of 465 nm blue LED were administered on the surface of V1 to induce antidromic spikes (see above). Success of antidromic activation was defined by two criteria. First, the probability of observing at least one spike within 5 ms from the onset of LED needed to be

greater than 20%. Second, the standard deviation of the timing of the first spikes within the 5 ms needed to be less than 0.5 ms.

Classification of saccade direction

We classified the direction of saccades and pseudo-saccades using linear discriminant analysis (LDA) and logistic regression on the number of spikes elicited by each single unit within 100 ms from the onset of each event. The procedure was preceded by principle component analysis (PCA) for dimensionality reduction. Only single units with average *fr* above 1 Hz was used. For each event of saccades or pseudo-saccades, the classifier assigned either nasal or temporal direction.

Training data consisted of the response to selected pseudo-saccades. This set of pseudo-saccades was selected such that the amplitudes and the number of events for nasal and temporal directions were matched. This ensured that the classifier depended on direction selectivity of each unit, rather than the difference in pseudo-saccade amplitudes or frequencies. The training data set was first subjected to PCA. Using the first dimensions that cumulatively accounted for 75% of total explained variance, we then trained LDA and logistic regression for classification. The resulting models for PCA, LDA, and regression were applied to the test data set, which were either responses to real saccades or pseudo-saccades whose amplitudes and directions had been matched to the real saccades.

As the same set of pseudo-saccades was presented to each animal during the recording (about 350 per animal, see Methods section on visual stimulation), we pooled data from single units across different animals for the same pseudo-saccade for the training data set. On the other hand, for the test data set, saccade data or the matched pseudo-saccade data from different animals were pooled simply based on the direction without regards to the amplitude. This is due to the difficulty in obtaining saccades of matching amplitudes from multiple animals. To mitigate the performance biases resulting from a specific pooling combination, five different combinations were generated. This pooling procedure potentially underestimates the performance of the classifier. Nonetheless, our focus was the comparison of the performance on saccades versus pseudo-saccades, both of which were subjected to the same procedure.

In order to calculate the classifier performance as a function of the number of single units used for the classification, a random subset of units (5, 10, 15, 20, 30, 40, 50, 100, 175, or 250 units) was chosen from the pooled data without replacement, before being subjected to training and testing. The entire procedure of the classification, including the random selection of units, was

repeated 10 times for each number of units for every pooling combination (5, see above), and the average performance was calculated (i.e., average of 5 x 10 = 50 results). An exponential function, forced to go through 50% accuracy with 0 units, was fit to the data points for visualization.

References

1. Crapse, T. B. & Sommer, M. A. Corollary discharge across the animal kingdom. *Nat. Rev. Neurosci.* **9**, 587–600 (2008).
2. Land, M. F. The Evolution of Gaze Shifting Eye Movements. *Curr. Top. Behav. Neurosci.* **41**, 3–11 (2019).
3. Land, M. F. Eye movements in man and other animals. *Vision Res.* **162**, 1–7 (2019).
4. Land, M. F. Eye movements of vertebrates and their relation to eye form and function. *J. Comp. Physiol. A Neuroethol. Sensory, Neural, Behav. Physiol.* **201**, 195–214 (2014).
5. Zuber, B. & Stark, L. Saccadic suppression: Elevation of visual threshold associated with saccadic eye movements. *Exp. Neurol.* **16**, 65–79 (1966).
6. Diamond, M. R., Ross, J. & Morrone, M. C. Extraretinal Control of Saccadic Suppression. *J. Neurosci.* **20**, 3449–3455 (2000).
7. Volkmann, F. C. Human visual suppression. *Vision Res.* **26**, 1401–1416 (1986).
8. Beeler, G. W. Visual threshold changes resulting from spontaneous saccadic eye movements. *Vision Res.* **7**, 769–775 (1967).
9. Matin, E. Saccadic suppression: A review and an analysis. *Psychol. Bull.* **81**, 899–917 (1974).
10. Chen, C. Y. & Hafed, Z. M. A neural locus for spatial-frequency specific saccadic suppression in visual-motor neurons of the primate superior colliculus. *J. Neurophysiol.* **117**, 1657–1673 (2017).
11. Sperry, R. W. Neural basis of the spontaneous optokinetic response produced by visual inversion. *J. Comp. Physiol. Psychol.* **43**, 482–9 (1950).
12. von Holst, E. & Mittelstaedt, H. The reafference principle. *Naturwissenschaften* **37**, 464–467 (1950).
13. Bremmer, F., Kubischik, M., Hoffmann, K. P. & Krekelberg, B. Neural dynamics of saccadic suppression. *J. Neurosci.* **29**, 12374–12383 (2009).
14. Goldberg, M. E. & Wurtz, R. H. Activity of superior colliculus in behaving monkey. I. Visual receptive fields of single neurons. *J. Neurophysiol.* **35**, 542–559 (1972).
15. Duffy, F. H. & Lombroso, C. T. Electrophysiological evidence for visual suppression prior to the onset of a voluntary saccadic eye movement. *Nature* **218**, 1074–1075 (1968).
16. Wurtz, R. H. Neuronal mechanisms of visual stability. *Vision Res.* **48**, 2070–2089 (2008).
17. Thiele, A., Henning, P., Kubischik, M. & Hoffmann, K. P. Neural mechanisms of saccadic suppression. *Science* **295**, 2460–2462 (2002).
18. Crowder, N. A., Price, N. S. C., Mustari, M. J. & Ibbotson, M. R. Direction and contrast tuning of macaque MSTd neurons during saccades. *J. Neurophysiol.* **101**, 3100–3107 (2009).
19. McFarland, J. M., Bondy, A. G., Saunders, R. C., Cumming, B. G. & Butts, D. A. Saccadic modulation of stimulus processing in primary visual cortex. *Nat. Commun.* **6**, 8110 (2015).

20. Zanos, T. P., Mineault, P. J., Guitton, D. & Pack, C. C. Mechanisms of Saccadic Suppression in Primate Cortical Area V4. *J. Neurosci.* **36**, 9227–9239 (2016).

21. Ibbotson, M. R., Price, N. S. C., Crowder, N. A., Ono, S. & Mustari, M. J. Enhanced motion sensitivity follows saccadic suppression in the superior temporal sulcus of the macaque cortex. *Cereb. Cortex* **17**, 1129–1138 (2007).

22. Price, N. S. C., Ibbotson, M. R., Ono, S. & Mustari, M. J. Rapid processing of retinal slip during saccades in macaque area MT. *J. Neurophysiol.* **94**, 235–246 (2005).

23. Berman, R. A., Cavanaugh, J., McAlonan, K. & Wurtz, R. H. A circuit for saccadic suppression in the primate brain. *J. Neurophysiol.* **117**, 1720–1735 (2017).

24. Sakatani, T. & Isa, T. Quantitative analysis of spontaneous saccade-like rapid eye movements in C57BL/6 mice. *Neurosci. Res.* **58**, 324–331 (2007).

25. Samonds, J. M., Geisler, W. S. & Priebe, N. J. Natural image and receptive field statistics predict saccade sizes. *Nat. Neurosci.* **21**, 1591–1599 (2018).

26. Corazza, R. & Lombroso, C. T. The neuronal dark discharge during eye movements in awake 'encéphale isolé' cats. *Brain Res.* **34**, 345–359 (1971).

27. Feldman, M. & Cohen, B. Electrical activity in the lateral geniculate body of the alert monkey associated with eye movements. *J. Neurophysiol.* **31**, 455–466 (1968).

28. Jeannerod, M. & Putkonen, P. T. S. Lateral geniculate unit activity and eye movements: Saccade-locked changes in dark and in light. *Exp. Brain Res.* **13**, 533–546 (1971).

29. Roth, M. M. *et al.* Thalamic nuclei convey diverse contextual information to layer 1 of visual cortex. *Nat. Neurosci.* **19**, 299–307 (2016).

30. Nakamura, H., Hioki, H., Furuta, T. & Kaneko, T. Different cortical projections from three subdivisions of the rat lateral posterior thalamic nucleus: A single-neuron tracing study with viral vectors. *Eur. J. Neurosci.* **41**, 1294–1310 (2015).

31. Bennett, C. *et al.* Higher-Order Thalamic Circuits Channel Parallel Streams of Visual Information in Mice. *Neuron* **102**, 477-492.e5 (2019).

32. Jennings, J. H. *et al.* Distinct extended amygdala circuits for divergent motivational states. *Nature* **496**, 224–228 (2013).

33. Sato, T. K., Häusser, M. & Carandini, M. Distal connectivity causes summation and division across mouse visual cortex. *Nat. Neurosci.* **17**, 30–32 (2014).

34. Zhang, S.-J. *et al.* Optogenetic Dissection of Entorhinal-Hippocampal Functional Connectivity. *Science* **340**, 1232627 (2013).

35. Rajkai, C. *et al.* Transient cortical excitation at the onset of visual fixation. *Cereb. Cortex* **18**, 200–209 (2008).

36. Crevecoeur, F. & Kording, K. P. Saccadic suppression as a perceptual consequence of efficient sensorimotor estimation. *Elife* **6**, 1–15 (2017).

37. Berman, R. A. & Wurtz, R. H. Functional identification of a pulvinar path from superior colliculus to cortical area MT. *J. Neurosci.* **30**, 6342–6354 (2010).

38. Lyon, D. C., Nassi, J. J. & Callaway, E. M. A disynaptic relay from superior colliculus to

dorsal stream visual cortex in macaque monkey. *Neuron* **65**, 270–279 (2010).

39. Castet, E. & Masson, G. S. Motion perception during saccadic eye movements. *Nat. Neurosci.* **3**, 177–183 (2000).

40. Watson, T. L. & Krekelberg, B. The Relationship between Saccadic Suppression and Perceptual Stability. *Curr. Biol.* **19**, 1040–1043 (2009).

41. Watson, T. & Krekelberg, B. An Equivalent Noise Investigation of Saccadic Suppression. *J. Neurosci.* **31**, 6535–6541 (2011).

42. Wurtz, R. H. Visual cortex neurons: response to stimuli during rapid eye movements. *Science* **162**, 1148–1150 (1968).

43. Wurtz, R. H. Comparison of effects of eye movements and stimulus movements on striate cortex neurons of the monkey. *J. Neurophysiol.* **32**, 987–994 (1969).

44. Ruiz, O. & Paradiso, M. A. Macaque V1 representations in natural and reduced visual contexts: Spatial and temporal properties and influence of saccadic eye movements. *J. Neurophysiol.* **108**, 324–333 (2012).

45. Kayama, Y., Riso, R. R., Bartlett, J. R. & Doty, R. W. Luxotonic responses of units in macaque striate cortex. *J. Neurophysiol.* **42**, 1495–1517 (1979).

46. Hopkins Duffy, F. & Lee Burchfiel, J. Eye movement-related inhibition of primate visual neurons. *Brain Res.* **89**, 121–132 (1975).

47. Kagan, I., Gur, M. & Snodderly, D. M. Saccades and drifts differentially modulate neuronal activity in V1: Effects of retinal image motion, position, and extraretinal influences. *J. Vis.* **8**, 1–25 (2008).

48. Laramée, M.-E. & Boire, D. Visual cortical areas of the mouse: comparison of parcellation and network structure with primates. *Front. Neural Circuits* **8**, 149 (2014).

49. Idrees, S., Baumann, M. P., Franke, F., Münch, T. A. & Hafed, Z. M. Perceptual saccadic suppression starts in the retina. *Nat. Commun.* **11**, 1–19 (2020).

50. Reppas, J. B., Usrey, W. M. & Reid, R. C. Saccadic eye movements modulate visual responses in the lateral geniculate nucleus. *Neuron* **35**, 961–974 (2002).

51. Burr, D. C., Morrone, M. C., Rosst, J. & Zeno, V. S. Selective suppression of the magnocellular visual pathway during saccadic eye movements. *Nature* **371**, 511–513 (1994).

52. Liu, B.-H., Huberman, A. D. & Scanziani, M. Cortico-fugal output from visual cortex promotes plasticity of innate motor behaviour. *Nature* **538**, 383–387 (2016).

53. Kleiner, M. *et al.* What's new in Psychtoolbox-3? *Perception* **36**, S14 (2007).

54. Brainard, D. H. The Psychophysics Toolbox. *Spat. Vis.* **10**, 433–436 (1997).

55. Pelli, D. G. The VideoToolbox software for visual psychophysics: Transforming numbers into movies. *Spat. Vis.* **10**, 437–442 (1997).

56. Pachitariu, M., Steinmetz, N., Kadir, S., Carandini, M. & Kenneth D., H. Kilosort: realtime spike-sorting for extracellular electrophysiology with hundreds of channels. *bioRxiv* 061481 (2016). doi:10.1101/061481

Acknowledgements

We thank M. Mukundan, J. Evora, N. Kim, Y. Li, B. Wong, and L. Bao for technical assistance and the former and current members of the Scanziani lab for comments and discussion. This investigation has been aided by a grant from The Jane Coffin Childs Memorial Fund for Medical Research and the Japan Society for the Promotion of Science to S.K.M and NIH grant U19NS107613 to M.S. M.S. is an investigator of the Howard Hughes Medical Institute.

Author contributions

S.K.M. and M.S. designed the study. S.K.M. conducted all experiments and analyses. S.K.M. and M.S. wrote the manuscript.

Main Figure Legends

Figure 1: Scrambling of direction selectivity in V1 during saccades

a, Schematic of experimental setup.

b, Overlay of two snapshots of the right eye (mirror image), taken before (red pupil) and after (blue pupil) a nasal saccade. Arrow indicates direction of saccade. N nasal; T, temporal.

c, Example traces of the eye position over 1-minute. Top trace, azimuth, up is nasal; bottom trace, elevation, up is dorsal.

d, Example traces of relative azimuthal eye position for nasal and temporal saccades.

e, Left, schematic of V1 recording during saccades on a vertical grating. Right, example neuron preferring nasal saccades. Average eye position for nasal and temporal saccades (top; shaded area, average ± standard deviation), raster plots (center), and PETH (bottom).

f, Left, scatter plot of the response to nasal and temporal saccades (average spike count in a 100 ms window from saccade onset), for all responsive neurons (see Methods). Blue, prefer nasal saccades; red, prefer temporal saccades; gray, no statistical difference; green, example neuron in (**e**). Significance determined by rank-sum test, $p < 0.05$ cutoff. Right, average PETH of discriminating neurons (colored data points in left scatter plot; $n = 97$ neurons, 4 mice), for preferred and non-preferred directions. Baseline normalized (see Methods). Shaded area, average ± standard error of the mean (s.e.m.).

g, Left, schematic of V1 recording during pseudo-saccades. Right, example neuron preferring temporal pseudo-saccades (otherwise as in (**e**)).

h, Left, scatter plot of response to nasal and temporal pseudo-saccades. Right, average PETH of discriminating neurons ($n = 44$ neurons, 4 mice; otherwise as in (**f**)).

i, Comparison of the response to saccades and pseudo-saccades.

j, Scatter plot of direction selectivity for real and pseudo-saccades for all neurons discriminating pseudo-saccade directions. Negative values, prefers temporal; positive values, prefers nasal (see Methods). Note poor correlation. Pearson $\rho = 0.22$, $p = 0.14$, $n = 44$ neurons, 4 mice.

k, Neurons sorted according to their direction selectivity for pseudo-saccades (lighter shade), overlaid with direction selectivity for real saccades (darker shade). Note the scrambling.

l, Classification accuracy of direction of motion (nasal or temporal) of a linear classifier trained on pseudo-saccades and tested on pseudo-saccades and real saccades, as a function of the number of neurons included in the analysis (see Methods for details). Lines, exponential fits. Note reduced accuracy on real saccades.

Figure 2: V1 receives non-visual input during saccades

a, Left, schematic of V1 recording during saccades on a gray screen. Right, example neuron preferring temporal saccades. Raster plots (top) and PETH (bottom).

b, Left, scatter plot of the response to nasal and temporal saccades for all responsive neurons. Blue, prefers nasal saccades; red, prefers temporal saccades; gray, no statistical difference; green, example neuron in (**a**). Right, Average PETH of discriminating neurons (colored data points in left scatter plot) for preferred and non-preferred directions (n = 109 neurons, 4 mice). Baseline normalized. Shaded area, average ± s.e.m.

c-d, Same as in **a-b**, but for saccades in TTX-blinded animals. **d**, right, n = 64, 8 mice.

e, Venn diagram of the number of neurons that respond to pseudo-saccades, saccades on a gray screen, and both. Percentages are out of the entire population.

f, Scatter plot of direction selectivity for pseudo-saccades (x-axis) against saccades on a gray screen (y-axis), for neurons that respond to both (79 neurons in (**e**)). Pearson ρ = 0.024, p = 0.84, n = 79 neurons, 4 mice.

g, Left, schematic of the linear regression-based model used to predict the number of spikes evoked by saccades on a vertical grating based on the response of neurons to pseudo-saccades and to saccades on a gray screen. Right, predicted number of spikes (x-axis) plotted against the observed values (y-axis).

Figure 3: The pulvinar provides non-visual saccade input to V1

a, Left, schematic of dLGN recording during saccades in TTX-blinded animals. Right, average PETH for preferred and non-preferred directions (*n* = 49 neurons, 4 mice). Shaded area, average ± s.e.m.

b, Left schematic of V1 recording during saccades under dLGN silencing. Right, average PETH for preferred and non-preferred directions (*n* = 56 neurons, 4 mice). Shaded area, average ± s.e.m.

c, Left, schematic of pulvinar recording during saccades in TTX-blinded animals. Right, example neuron preferring temporal saccades. Raster plots (top), and PETH (bottom).

d, Left, scatter plot of the response to nasal and temporal saccades (for all responsive neurons). Right, average PETH of discriminating neurons (colored data points on left scatter plot) for preferred and non-preferred directions (*n* = 61 neurons, 12 mice). Baseline normalized. Shaded area, average ± s.e.m.

e, Left, Schematic of pulvinar recordings during saccades in TTX-blinded animal and optogenetic antidromic activation of pulvinar projections to V1. Center, example of antidromically activated neuron. Raster plot (top) and spike probability (bottom; 0.05 ms bin). Blue shaded area indicates time of the 1-ms LED illumination. Right, response of neuron shown in center panel to saccades. This neuron prefers nasal saccades. Raster plot (top) and PETH (bottom).

f, Average PETH of saccade-responsive pulvinar neurons that were antidromically activated by illumination of V1 (*n* = 13 neurons, 3 mice). Shaded area, average ± s.e.m.

g, Left, schematic of V1 recording during saccades in TTX-blinded mice before and after pulvinar silencing. Center, raster plot (top) and PETH (bottom) of an example neuron in response to nasal saccades before and after pulvinar silencing. Right, average PETH of saccade responsive neurons before and after pulvinar silencing (*n* = 56 neurons, 5 mice). All nasal and temporal saccades are included. Shaded area, average ± s.e.m.

h, LFP from example animal aligned to the time of saccades for layer 2/3 (L2/3), layer 5 (L5) and layer 6 (L6) before and after pulvinar silencing.

Figure 4: The pulvinar scrambles direction selectivity in V1 during saccades

a, Left, schematic of V1 recording during pseudo-saccades. Center, average PETH for all pseudo-saccade responsive neurons to nasal and temporal directions, baseline normalized (n = 102 neurons, 9 mice). Shaded area, average ± s.e.m. Right, average PETH of single neurons that discriminate nasal and temporal pseudo-saccades, sorted by their preferred and non-preferred pseudo-saccade directions (n = 29 neurons). Shaded area, average ± s.e.m.

b, Same as in (**a**), but for real saccade responses recorded after pulvinar silencing in the same animals. Center, n = 135 neurons; right, n = 53 neurons.

c, Left, comparison of the response to saccades and pseudo-saccades. Center, scatter plot of direction selectivity for real and pseudo-saccades for all neurons discriminating pseudo-saccade direction. Pearson $\rho = 0.72$, $p < 0.0001$, 29 neurons, 9 animals. Note good correlation. Right, neurons sorted according to their direction selectivity for pseudo-saccades (lighter shade), overlaid with direction selectivity for real saccades (darker shade).

d, Left, classification accuracy of direction of motion (nasal or temporal) of a linear classifier trained on pseudo-saccades and tested on pseudo-saccades and real saccades, as a function of neurons included in the analysis. Lines, exponential fits. Note equally good accuracy on pseudo- and real saccades. Right, classification accuracy for real saccades under control condition (black, from Fig. 1l) and under pulvinar silencing (magenta), for comparison.

e, The integration of non-visual input from the pulvinar with saccade-induced visual motion results in scrambling of direction selectivity of V1 neurons during saccades.

Extended Data Figure Legends

Extended Data Figure 1: Distribution of real and pseudo-saccade amplitudes

a, Histogram of saccade amplitudes in control mice. Blue, nasal saccades; red, temporal saccades. Bars indicate 25% and 75% quartile range, dot denotes median. Nasal saccades: median, 13.2°; 25% quartile, 9.9°; 75% quartile, 16.2°; *n* = 296. Temporal saccades: median 7.9°; 25% quartile, 6.2°; 75% quartile, 10.26°; temporal, *n* = 189. 4 mice.

b, Histogram of pseudo-saccade amplitudes. For analyses, pseudo-saccades with amplitudes matched to real saccades were further selected for each animal. All animals were presented with the same pseudo-saccades. Nasal pseudo-saccades: median, 12.5°; 25% quartile, 9.6°; 75% quartile, 15.8°; *n* = 193. Temporal pseudo-saccades: median 9.4°; 25% quartile, 6.7°; 75% quartile, 11.6°; *n* = 207.

c, Same as in (**a**) but for TTX-blinded animals. Nasal saccades: median, 13.9°; 25% quartile, 11.2°; 75% quartile, 17.5°; *n* = 887. Temporal saccades: median 8.8°; 25% quartile, 6.5°; 75% quartile, 11.5°; temporal, *n* = 561. 8 mice.

d, Same as in (**a**) but for animals with the pulvinar silenced. °Nasal saccades: median, 13.3°; 25% quartile, 10.4°; 75% quartile, 16.3°; *n* = 579. Temporal saccades: median 9.0°; 25% quartile, 6.9°; 75% quartile, 11.4°; temporal, *n* = 329. 9 mice.

884 **Extended Data Figure 2: Dependence of saccade and pseudo-saccade response on spike**
885 **waveform and cortical depth**

886 **a,** Left, schematic of V1 recording during saccades on a vertical grating. Right, average PETH of
887 saccade responsive neurons to nasal and temporal saccades. Baseline normalized. Shaded area,
888 average ± s.e.m.

889 **b,** Cumulative distribution function (CDF) of direction discriminability (absolute value of direction
890 selectivity, see Methods), plotted for all regular-spiking (RS) and fast-spiking (FS) neurons.
891 Anderson-Darling test, $p = 0.28$, $n = 268$ for RS, 49 for FS, 4 mice. Inset, median spike shape
892 normalized to the trough. Shaded area, 25% and 75% quartiles.

893 **c,** Left, average PETH of all neurons to saccades. All nasal and temporal saccades are included.
894 $n = 30$ for layer 2/3, 52 for layer 4, 135 for layer 5, and 95 for layer 6. Baseline normalized. Shaded
895 area, average ± s.e.m. Center, scatter plot of direction discriminability (x-axis) of all units as a
896 function of cortical depth (y-axis). Open circles, statistically non-significant; filled, significant (cutoff
897 $p < 0.05$, Wilcoxon rank-sum test). Color code as in left. Right, CDF of discriminability by cortical
898 depth. Layers 2/3 and 4 were concatenated. 3-sample Anderson-Darling test, $p < 0.0001$.

899 **d-f,** same as **a-c** but for pseudo-saccade responses in the same neurons. Note *n* is the same as
900 **a-c**. **e**, Anderson-Darling test, $p = 0.065$. **f**, right, 3-sample Anderson-Darling test, $p = 0.12$.

901

902

903

904

905

906

907

908

909

910

911

912

Extended Data Figure 3: Direction selectivity for saccade-inducted motion and pseudo-saccades become correlated upon pulvinar silencing

a, Comparison of the response to saccades and pseudo-saccades in control. Right, scatter plot of direction selectivity for real and pseudo-saccades for all neurons that discriminate between nasal and temporal direction under either condition. Note the lack of a significant correlation (Pearson $\rho = 0.16$, $p = 0.081$, $n = 127$, 4 mice).

b, Same as in (**a**), but saccade response was recorded after pulvinar silencing. Right, direction selectivity became correlated (Pearson $\rho = 0.43$, $p = 0.00019$, $n = 70$, 8 mice).

Extended Data Figure 4: Dependence of saccade response on spike waveforms and cortical depth in TTX-blinded mice

a, Left, schematic of V1 recording during saccades in TTX-blinded animals. Right, current source density analysis from an example animal, showing a major sink in the superficial layers. Data from 89 nasal and 82 temporal saccades.

b, CDF of direction discriminability for RS and FS neurons. Anderson-Darling test, $p = 0.090$, $n = 175$ for RS, 28 for FS. Inset, median spike shape normalized to the trough. Shaded area, 25% and 75% quartiles.

c, Left, average PETH of all neurons to saccades. All nasal and temporal saccades are included. Layer 2/3, 13 neurons; layer 4, 24; layer 5, 107; layer 6, 59. Shaded area, average ± s.e.m. Center, scatter plot of direction discriminability of all units (x-axis) as a function of cortical depth (y-axis). Open circles, statistically non-significant; filled, significant (cutoff $p < 0.05$, Wilcoxon rank-sum test). Color code as in left. Right, CDF of discriminability by cortical depth. Layers 2/3 and 4 were concatenated. 3-sample Anderson-Darling test, $p < 0.0001$.

968 **Extended Data Figure 5: Intraocular injection of TTX abolishes visual response in V1**

969 **a,** Left, schematic of V1 recording during a brief (26 ms) full-field flash. Center, multi-unit response
970 from an example recording. Raster plot (top) and average PETH (bottom). Right, average PETH
971 of 4 mice. Baseline normalized. Shaded area, average ± s.e.m. 137.9 ± 31.2 Hz (22.1 ± 4.3%)
972 evoked *fr* ± s.e.m. in a 60 ms window post onset (from +10 ms post-onset to +70 ms).

973 **b,** Same as in (**a**), but in TTX-blinded animals (8 mice). Note the lack of visual response. -8.0 ±
974 15.4 Hz (0.12 ± 3%) evoked *fr* ± s.e.m. in the 60 ms window post onset. Wilcoxon rank-sum test,
975 one-tail, $p = 0.0020$.

976

977

978

979

980

981

982

983

984

985

986

987

988

989

990

991

992

993

Extended Data Figure 6: Modeling saccade response on a vertical grating with response to visual or non-visual inputs

Left, schematic of the linear regression-based model used to predict the number of spikes evoked by saccades on a vertical grating based on the response of neurons to pseudo-saccades and to saccades on a gray screen. Results from the sum of the two inputs are shown in the main figure. Center, predicted number of spikes from the response to pseudo-saccades (x-axis) plotted against the observed values (y-axis). The model explains 32% of the observed variance. Right, predicted number of spikes from the response to saccades on a gray screen (x-axis) plotted against the observed values (y-axis). The model explains 69% of the observed variance.

Extended Data Figure 7: The dLGN is not the source of non-visual saccade response in V1

a, Left, schematic of dLGN recording during saccades in TTX-blinded animals. Right, example neuron preferring temporal saccades. Raster plots (top) and PETH (bottom).

b, Left, average PETH of saccade responsive neurons to nasal and temporal saccades. *n* = 83, 4 mice. Baseline normalized. Shaded area, average ± s.e.m. Right, scatter plot of the response to nasal and temporal saccades (average spike count in a 100 ms window from saccade onset), for all responsive neurons. Blue, prefer nasal saccades; red, prefer temporal saccades; gray, no statistical difference; green, example neuron in (**a**).

c-d, Same as in **a-b**, but for V1 neurons under dLGN silencing in TTX-blinded animals. **d**, Left, *n* = 106, 4 mice. Right, Note direction selective neurons in V1 under dLGN silencing.

Extended Data Figure 8: Muscimol-BODIPY injection in the dLGN blocks visual response in V1

a, Left, schematic of V1 recording during a brief (32 ms) presentation of a full-field grating (see Methods). Center, multi-unit response from an example recording. Raster plot (top) and PETH (bottom). Right, average PETH of 3 mice. Baseline normalized. Shaded area, average ± s.e.m. 173.5 ± 29% average increase in evoked *fr* ± s.e.m.

b, Left and center, same as in (**a**), but for mice injected with muscimol-BODIPY in the dLGN. Right, average PETH of 4 mice. Recording started after muscimol injection. Response was measured both at the start of the recording session and at the end. Note the lack of visual response in both cases. Baseline normalized. Shaded area, average ± s.e.m. Average increase in evoked *fr* ± s.e.m. was -16.7 ± 7.5% (start) and 14.1 ± 8.8% (end).

c, Section images of the four mice injected with muscimol-BODIPY in the dLGN in (**b**). Red, BODIPY. Scale bar, 1 mm.

Extended Data Figure 9: Silencing the pulvinar eliminates non-visual saccade input in V1

a, Left, schematic of V1 recording during saccades in TTX-blinded animals before and after pulvinar silencing. Center, current source density (CSD) map of an example animal, prior to pulvinar silencing. All nasal and temporal saccades are included. Note the strong sink in the superficial layers. Right, CSD map of the same animal, but after the silencing. Color scale same as in the center panel. Not the attenuated sink.

b, Left, average PETH of discriminating neurons for preferred and non-preferred directions, prior to the pulvinar silencing. Right, average PETH of the same neurons, but after the pulvinar silencing. n = 29, 5 mice. Shaded area, average ± s.e.m.

c, Discriminability of the 29 neurons in (**b**), pre and post silencing of the pulvinar. Gray, individual animals; black, average.

Extended Data Figure 10: Direction selective response of V1 units to saccades under pulvinar silencing and to pseudo-saccades

a, Left, schematic of V1 recording during pseudo-saccades. Center, example neuron preferring temporal saccades. Raster plots (top) and PETH (bottom). Right, scatter plot of the response to nasal and temporal saccades (average spike count in a 100 ms window from saccade onset), for all responsive neurons. Blue, prefer nasal saccades; red, prefer temporal saccades; gray, no statistical difference; green, example neuron on the left.

b, Same as in (**a**), but for real saccade responses recorded after pulvinar silencing in the same animals. Center, example neuron preferring nasal saccades.

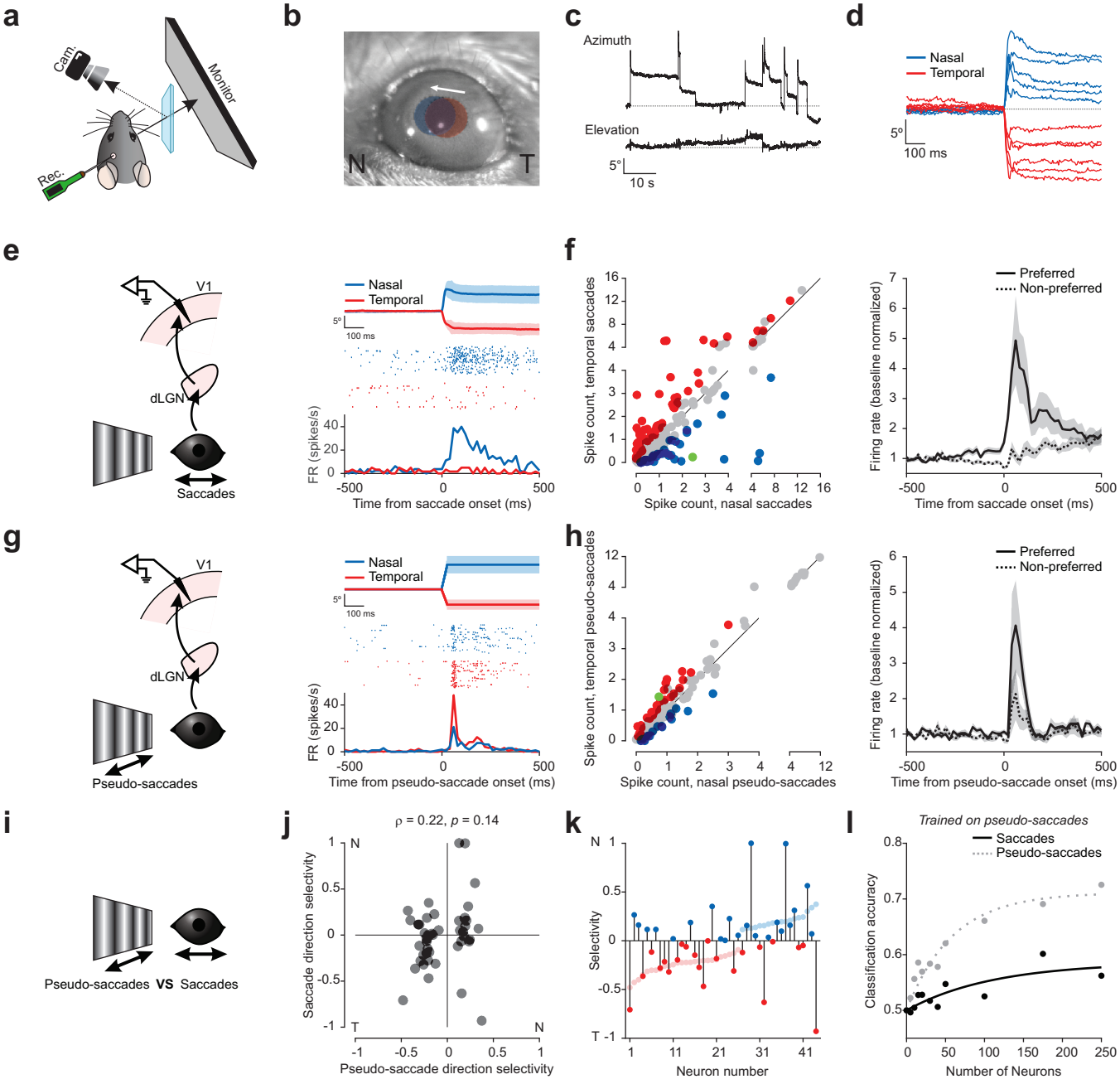

Fig. 1 | Scrambling of direction selectivity in V1 during saccades

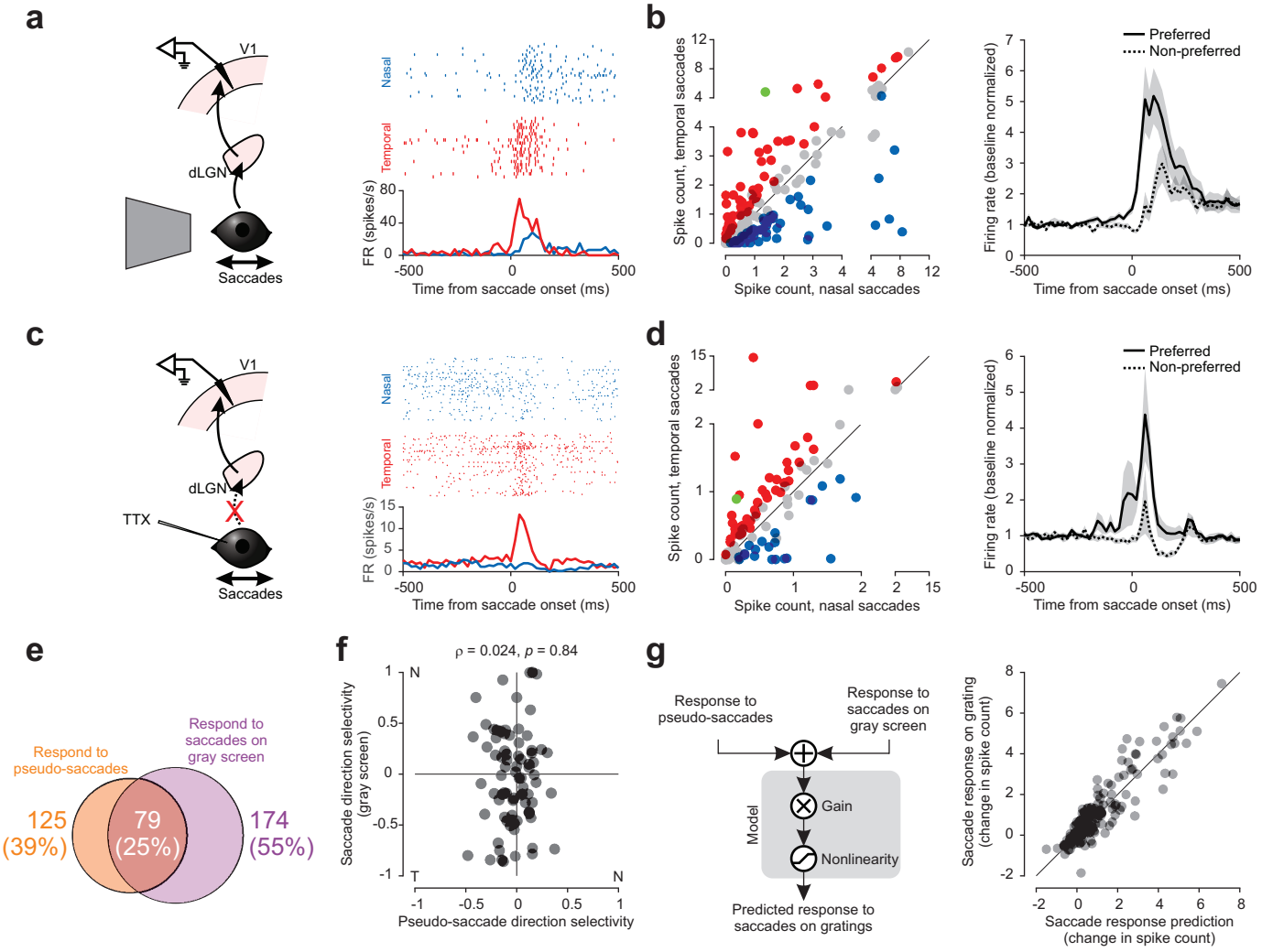

Fig. 2 | V1 receives non-visual input during saccades

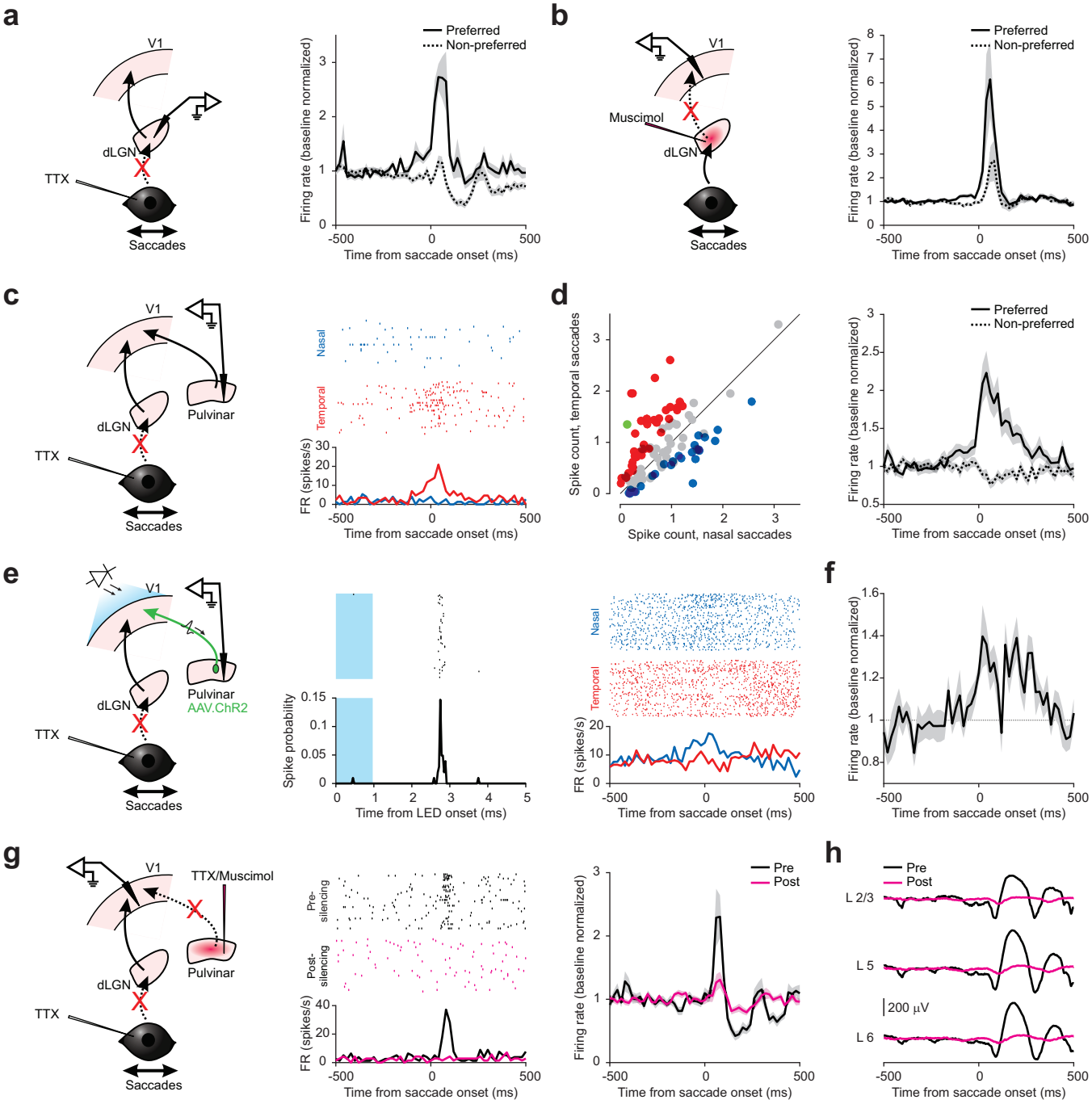

Fig. 3 | The pulvinar provides non-visual saccade input to V1

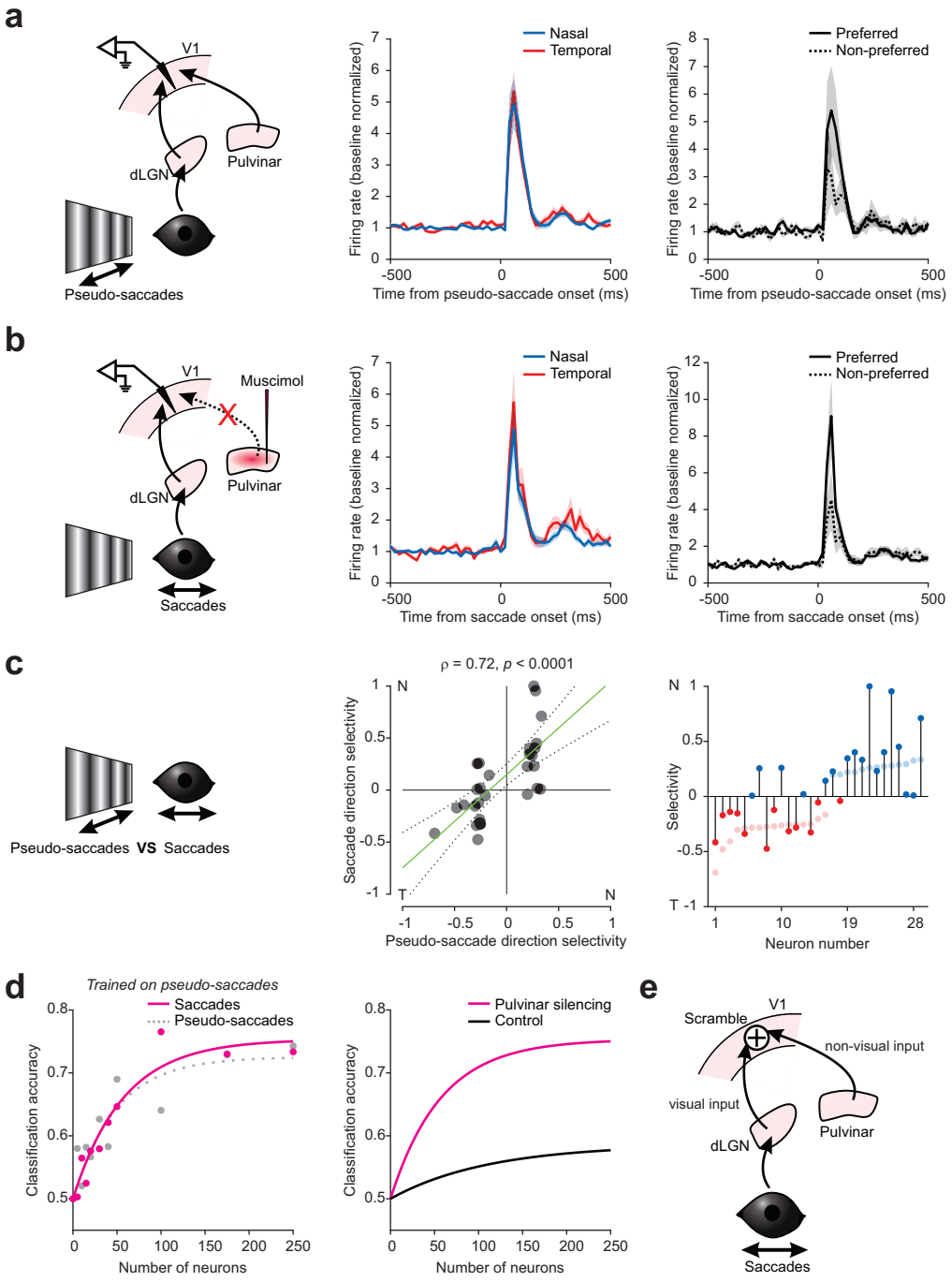

Fig. 4 | The pulvinar scrambles direction selectivity in V1 during saccades

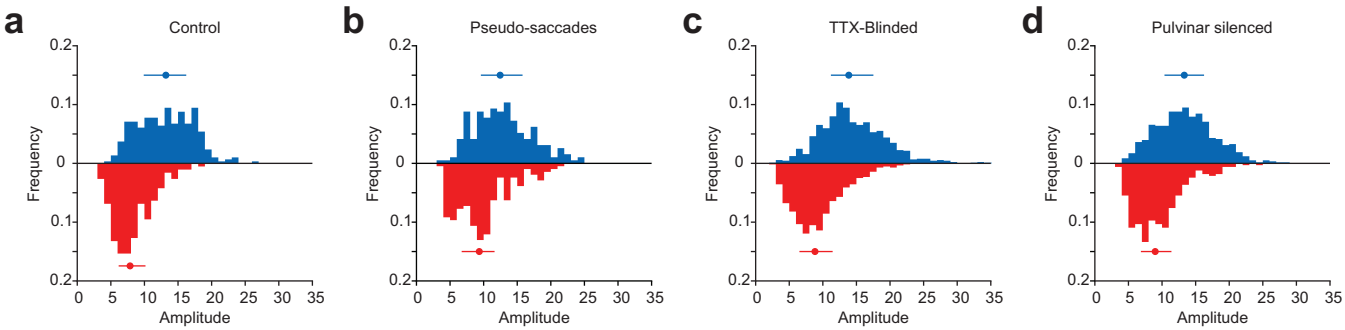

Extended Data Fig. 1 | Distribution of real and pseudo-saccade amplitudes

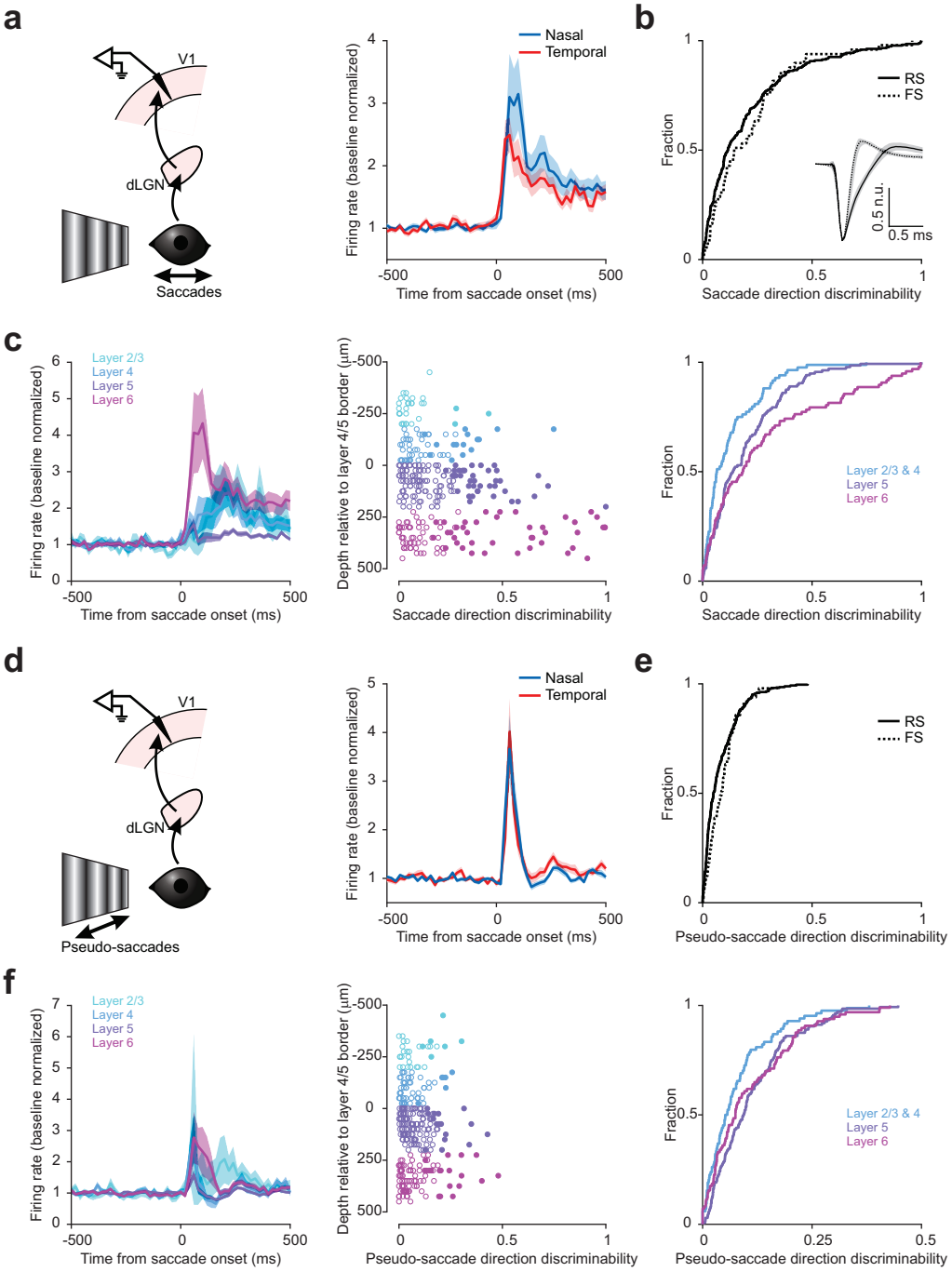

Extended Data Fig. 2 | Dependence of saccade and pseudo-saccade response on spike waveform and cortical depth

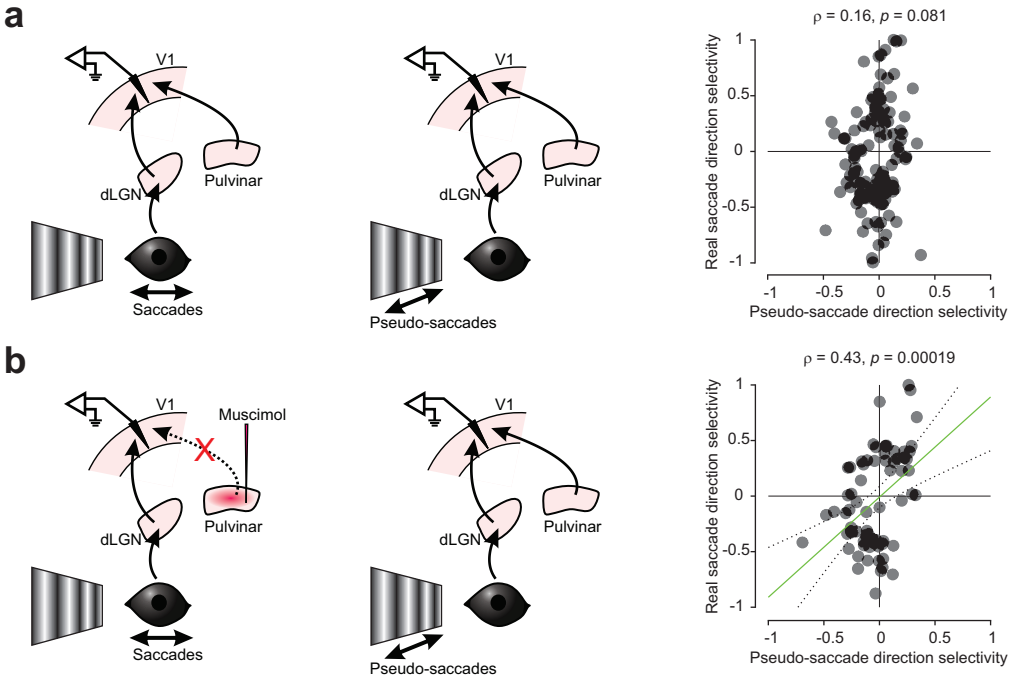

Extended Data Fig. 3 | Direction selectivity for saccade-induced motion and pseudo-saccades become correlated upon pulvinar silencing

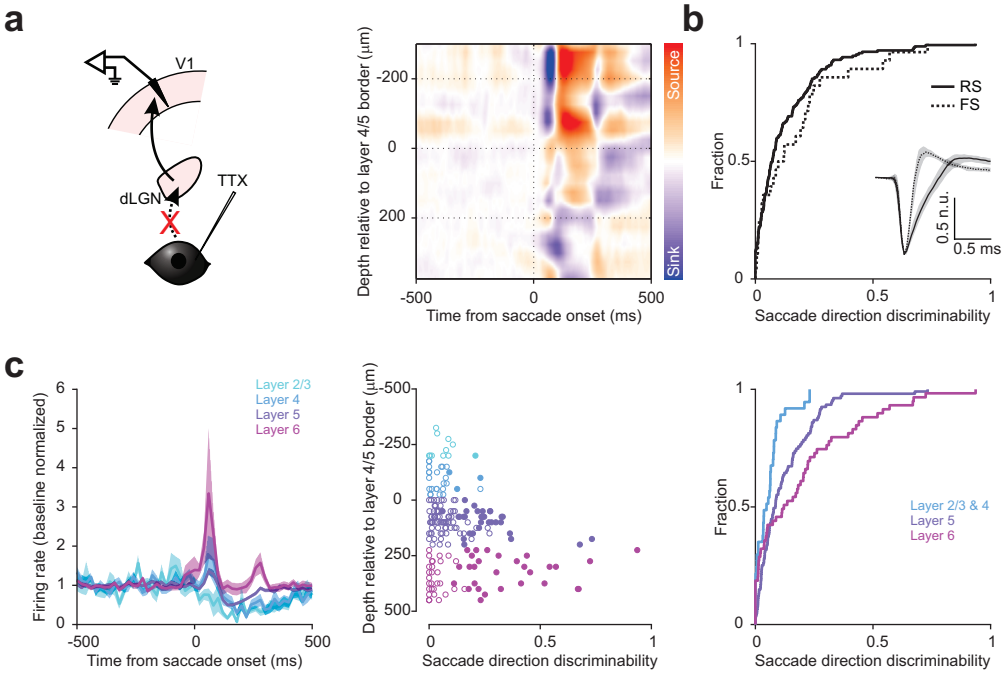

Extended Data Fig. 4 | Dependence of saccade response on spike waveforms and cortical depth in TTX-blinded mice

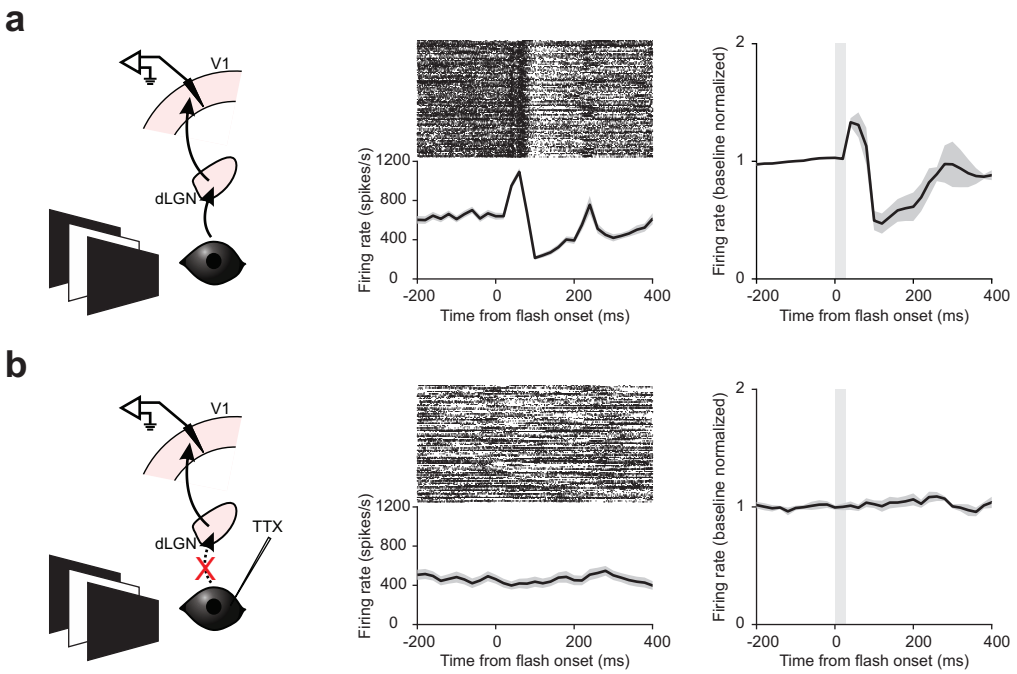

Extended Data Fig. 5 | Intraocular injection of TTX abolishes visual response in V1

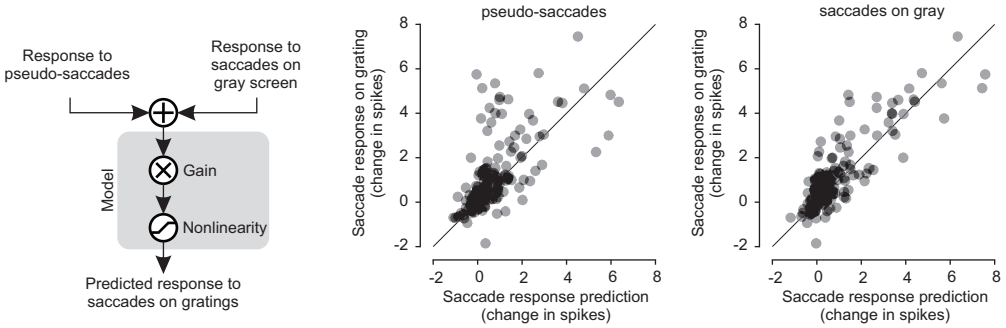

Extended Data Fig. 6 | Modeling saccade response on a vertical grating with respone to visual or non-visual input

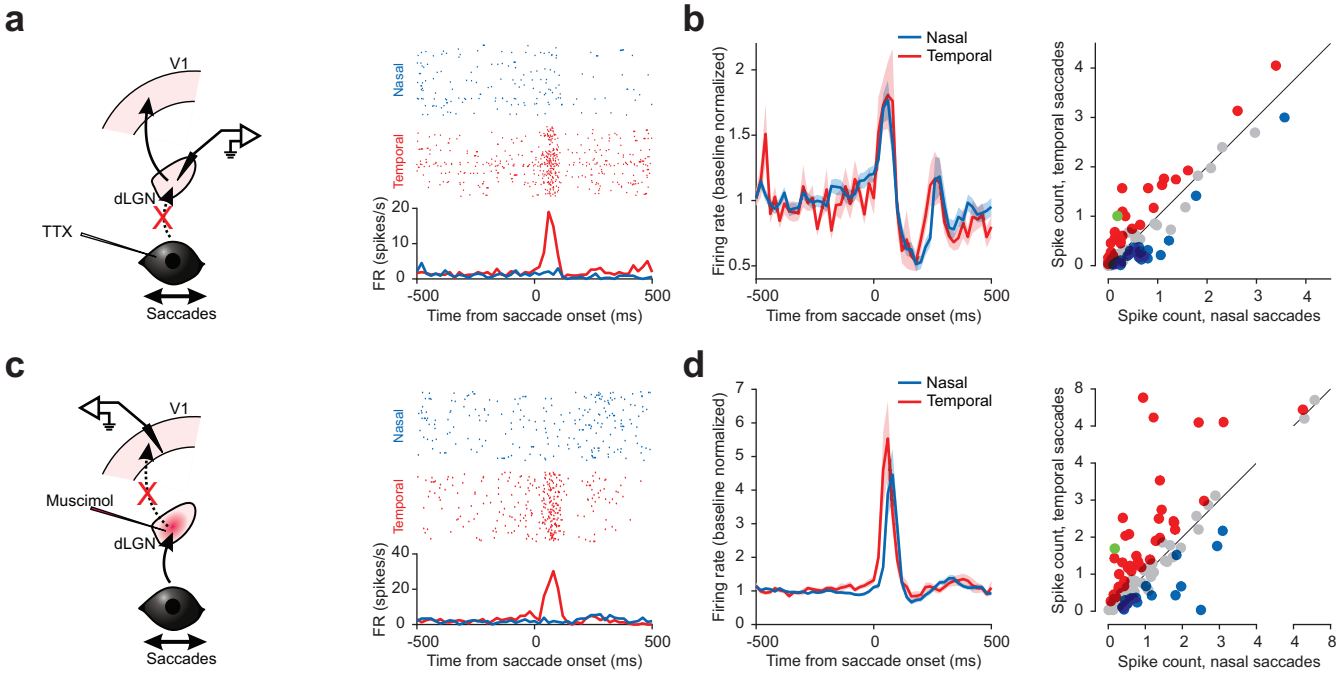

Extended Data Fig. 7 | The dLGN is not the source of non-visual saccade response in V1

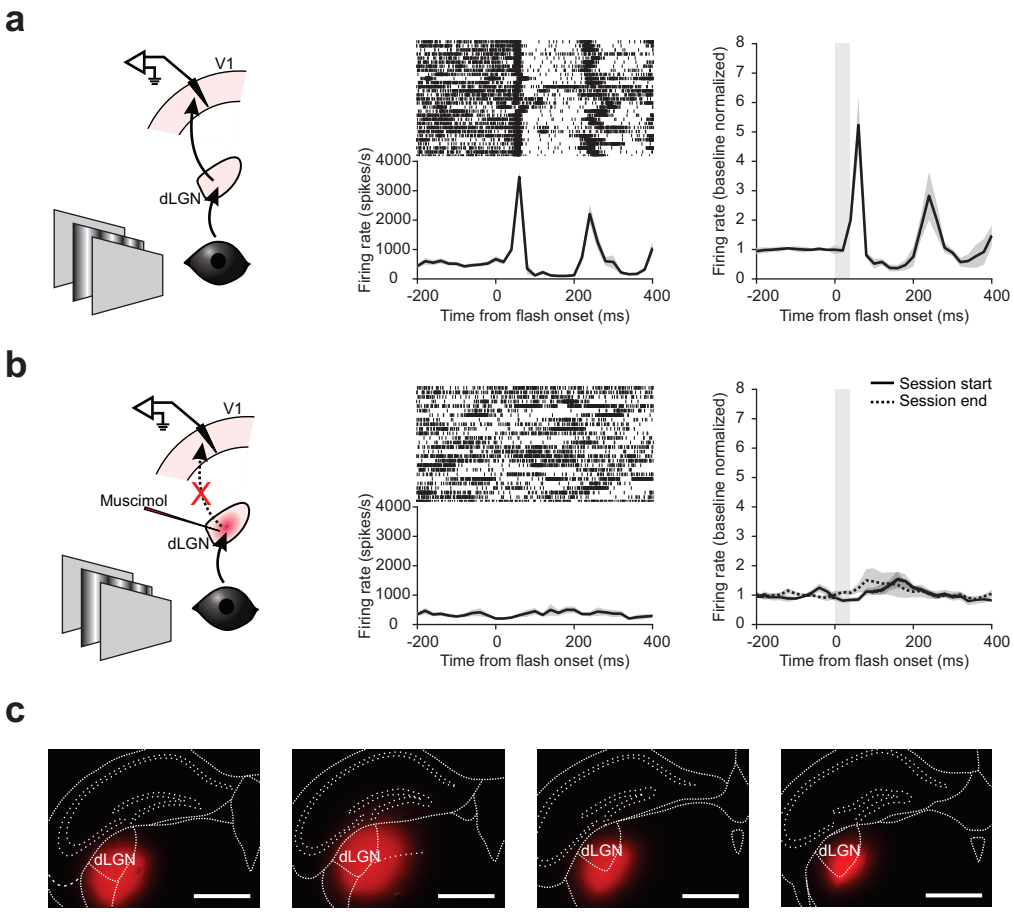

Extended Data Fig. 8 | Muscimol injection in the dLGN blocks visual responses in V1

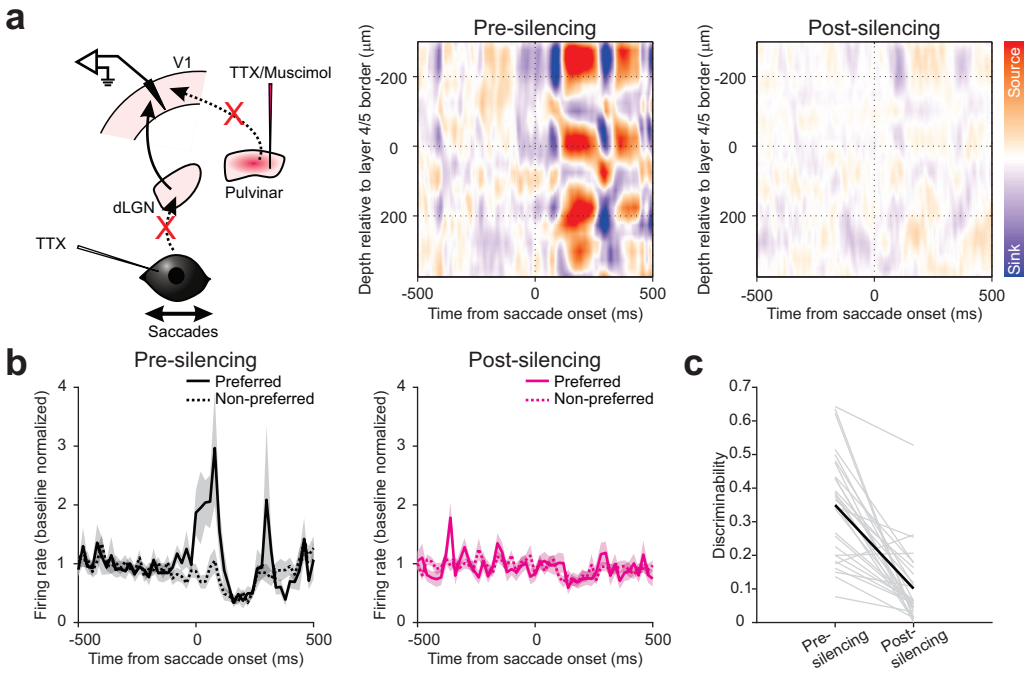

Extended Data Fig. 9 | Silencing the pulvinar eliminates non-visual saccade input in V1

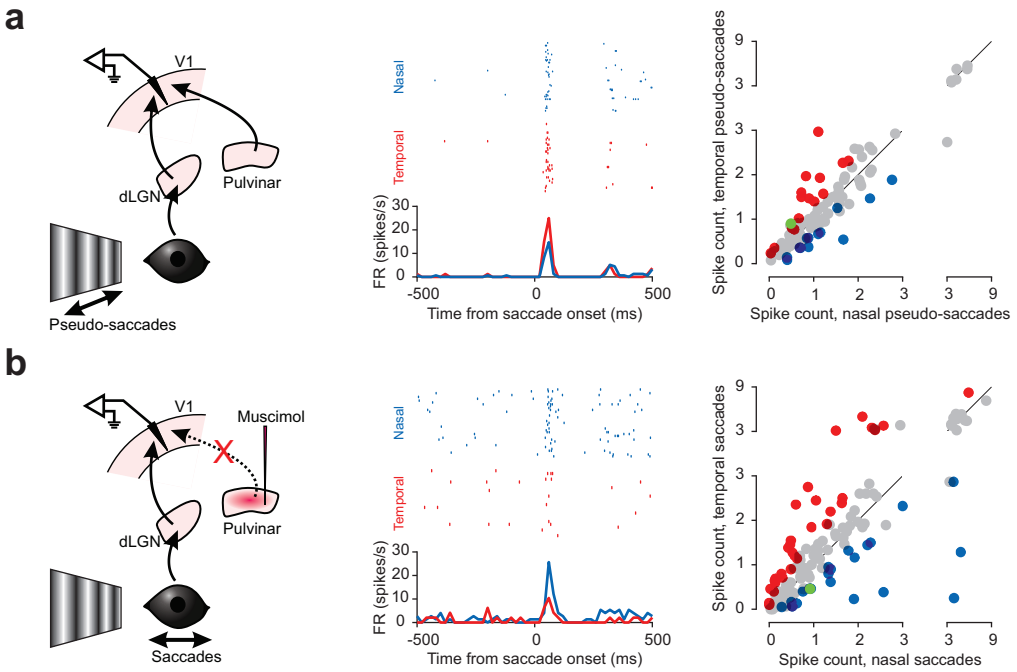

Extended Data Fig. 10 | Direction selective response of V1 neurons to saccades under pulvinar silencing and to pseudo-saccades